THE JOURNAL OF PHYSICAL CHEMISTRY B
A JOURNAL OF THE AMERICAN CHEMICAL SOCIETY

pubs.acs.org/JPCB

Article

# Multicomponent Quantum Mechanics/Molecular Mechanics Study of Hydrated Positronium

Mateus Bergami, Andre L. D. Santana, Jorge Charry Martinez, Andres Reyes, Kaline Coutinho, and Márcio T. do N. Varella*

Cite This: *J. Phys. Chem. B* 2022, 126, 2699–2714

Read Online

ACCESS | Metrics & More | Article Recommendations | Supporting Information



**ABSTRACT:** We propose a model for solvated positronium (Ps) atoms in water, based on the sequential quantum mechanics/molecular mechanics (s-QM/MM) protocol. We developed a Lennard-Jones force field to account for Ps−water interactions in the MM step. The repulsive term was obtained from a previously reported model for the solvated electron, while the dispersion constant was derived from the Slater−Kirkwood formula. The force field was employed in classical Monte Carlo (MC) simulations to generate Ps−solvent configurations in the *NpT* ensemble, while the quantum properties were computed with the any-particle molecular orbital method in the subsequent QM step. Our approach is general, as it can be applied to other liquids and materials. One basically needs to describe the solvated electron in the environment of interest to obtain the Ps solvation model. The thermodynamical properties computed from the MC simulations point out similarities between the solvation of Ps and noble gas atoms, hydrophobic solutes that form clathrate structures. We performed convergence tests for the QM step, with particular attention to the choice of basis set and expansion centers for the positronic and electronic subsystems. Our largest model was composed of the Ps atom and 22 water molecules in the QM region, corresponding to the first solvation shell, surrounded by 128 molecules described as point charges. The mean electronic and positronic vertical detachment energies were (4.73 ± 0.04) eV and (5.33 ± 0.04) eV, respectively. The latter estimates were computed with Koopmans' theorem corrected by second-order self-energies, for a set of statistically uncorrelated MC configurations. While the Hartree−Fock wave functions do not properly account for the annihilation rates, they were useful for numerical tests, pointing out that annihilation is more sensitive to the choice of basis sets and expansion centers than the detachment energies. We further explored a model with reduced solute cavity size by changing the Ps−solvent force field. Although the pick-off annihilation lifetimes were affected by the cavity size, essentially the same conclusions were drawn from both models.

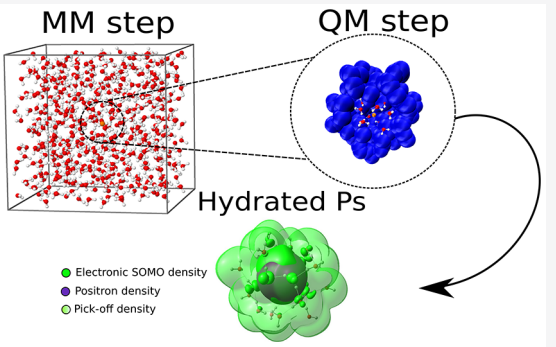


## 1. INTRODUCTION

Positrons and positronium (Ps) atoms are important nanoscale probes in materials sciences useful to investigate defects and pores in metals,[1] semiconductors,[2] polymers,[3,4] zeolites,[5] and other nano-/mesoporous materials.[6,7] The most widely employed technique is probably positron annihilation lifetime spectroscopy (PALS),[6,8,9] which seeks the signatures of free volumes and chemical environments in the $\gamma$ radiation produced by pair annihilation from quasi-free positrons, para-Ps (singlet spin coupling), and ortho-Ps (triplet coupling).

The interest in positronic interactions with soft matter has also increased in recent years.[10] PALS is now acknowledged as a useful tool to investigate the conformational, structural, and microenvironmental properties of biomimetic systems[11] as well as phase transitions of lipid bilayers[12] and pharmaceutically relevant compounds.[13,14] Positron emission tomography (PET) has also become a well-established imaging technique of living tissues,[15−17] and the Ps contribution to the annihilation signals is expected to provide a basis for further technological progress. For instance, the sensitivity of ortho-Ps lifetime to the concentration of molecular oxygen could probe the hypoxic regions in tumors,[18,19] and three-photon detection could determine the location of ortho-Ps annihilation in the tissue with improved accuracy.[20,21] Finally, positrons and Ps atoms are produced along the tracks of the heavy particles used in ion-beam cancer therapy,[22,23] and positron-based tumor treatments have also been proposed.[24,25]

The modeling of positrons and Ps interactions for medical applications often considers liquid water as a surrogate of human tissue.[22,26,27] The positrons are produced by $\beta^+$ decay

**Received:** November 26, 2021
**Revised:** March 18, 2022
**Published:** April 4, 2022

with energies around $10^2$ keV, so their thermalization involves a complex cascade of events. In liquids,[28] a fast positron induces ionization events producing energetic electrons which, in turn, further ionize the medium generating "spurs", i.e., nanovolumes containing electron−ion pairs. As the positron slows down, the spur domains get closer together, eventually giving rise to a terminal "blob", a region where the positron motion becomes diffusive. Electron−ion pairs are also present in the blob, where Ps formation takes place. Monte Carlo (MC) simulations pointed out that Ps formation reaches a maximum for positron energies around 20 eV,[22] although phenomenological arguments suggest that nearly thermalized particles give rise to bound electron−positron pairs.[28] The quasi-free Ps atoms are energetically stable against breakup into hydrated electrons and positrons,[29] and they thermalize through interactions with the surrounding molecules. The Ps formation yield in water[30,31] and in uterine human tissue[31] would be around and above 40% with respect to the initial number of positrons. The observed room-temperature annihilation lifetimes in water are 0.13 ns for para-Ps[30] and 1.85 ns for ortho-Ps,[30,32] although higher values were reported for human tissue.[31]

The thermalized Ps particles are often described with bubble models. The original formulation was proposed by Ferrel in 1957;[33] they assumed a Ps particle trapped in a "bubble", i.e., a spherically symmetric potential well arising from the exchange repulsion between the electron in the Ps and those in the neighboring molecules. The bubble radius was then estimated by minimizing the sum of the energy of the trapped Ps with the surface energy. The model was improved by Tao[34] and Eldrup et al.,[35] who considered a pointlike Ps confined by an infinite spherically symmetric potential barrier accounting for the repulsive interaction with the liquid. The wave function for the center of mass of the confined particle can be calculated analytically, as well as its overlap with the surrounding electrons, assumed to have a penetration thickness $\delta$ inside the confining potential. The pick-off annihilation rate, between the positron and the electrons in the neighboring molecules of the liquid, can be expressed in terms of the potential radius and the pick-off overlap thickness. Further refinements of the phenomenological approach, including finite confining potentials and finite-sized Ps particles, were reviewed by Stepanov et al.[28] (see also refs 36−38 for more recent developments).

A quantum mechanical model for solvated Ps was proposed by Chuev et al.[39,40] The exotic atom was described with density functional theory (DFT), and the solvent was treated within the integral equation theory (IET) framework. The most frequently used quantum mechanical approach to Ps in condensed media is the path integral Monte Carlo (PIMC) method.[41−45] Most of these studies addressed Ps atoms confined in polymer voids, although with different models for the Ps−material interaction. In particular, Schmitz et al.[41] performed molecular dynamics (MD) simulations for the polymers, followed by PIMC calculations with the Ps−polymer interaction described by atomistic potentials accounting for the Coulomb and dispersion interactions, while Bug et al.[45] considered a cavity in a polarizable medium, either empty or filled with fluid. In both studies, the annihilation rates were obtained from the electronic densities of the polymer[41] and the cavity-filling fluid[45] calculated with DFT.

In recent years, numerically efficient multicomponent methods, which can be applied to polyatomic positronic molecules,[46,47] became available. Solvation techniques, such as MD- and MC-based algorithms, are nowadays routinely employed for molecular liquids. We present a computational method to simulate hydrated Ps atoms that combine some of those techniques, in particular the sequential quantum mechanics/molecular mechanics (s-QM/MM) solvation method[48] and the any particle molecular orbital (APMO)[47] method for systems comprising more than a single quantum species. We propose a force field, combining Coulomb and Lennard-Jones (LJ) potentials to account for Ps−water and water−water atomic interactions, which allows for classical MC simulations of solvated Ps particles. The statistically uncorrelated Ps−solvent configurations generated by the MC procedure are subsequently employed in the APMO computations to obtain the QM properties of interest. While the classical step might sound at first inadequate for the light Ps atom, a similar approach has been employed for the solvated electron.[49] The bubble and quantum models outlined above assume that Ps is a hydrophobic species that essentially carves a cavity in the water bulk. This property is a consequence of the Pauli repulsion, which can be emulated by suitably chosen repulsive potentials in the classical simulations. The statistically uncorrelated MC configurations also account for thermodynamic properties, as they describe the equilibrated Ps−solvent system in the given statistical ensemble. In turn, the QM calculations describe the Ps and electrons of the neighboring water molecules at the same level, according to the APMO approximation of choice. The properly antisymmetrized wave functions are expected to consistently account for the pick-off annihilation rates, as recently pointed out by Marlotti et al.[38]

The interest in Ps solvation is renewed in view of its relevance to PET imaging and other biomedical applications. Detailed information on molecular-level processes is essential to model the positron tracks,[26,27,50−52] so the field should also profit from sophisticated atomistic models for Ps interactions. Our solvation method can be viewed as a step in that direction, and its adaptation to other environments, such as polymers and biomaterials, would be straightforward.

This paper is organized as follows. In section 2 we describe the s-QM/MM method, the classical simulations for the liquid phase, and the force field (FF) developed for Ps and summarize the APMO quantum techniques. In section 3 we describe the cluster models used to investigate some relevant numerical aspects and also present the s-QM/MM results. The conclusions and perspectives are outlined in section 4.

## 2. METHODS

As outlined above, our solvation model is based on the s-QM/MM protocol, which involves classical MC simulations (MM step) followed by quantum calculations exploring the statistically uncorrelated solute−solvent configurations (QM step). In the following, we describe the basic aspects of the MM simulations, including the force field for Ps−water interactions, as well as the APMO approximations employed in the QM calculations.

### 2.1. Classical Simulations and Ps−Water Force Field.

We performed MC simulations with the Metropolis algorithm implemented in the DICE software package[53] for a simulation box containing 500 water molecules and a single Ps atom. The geometries of the water molecules were kept rigid, such that only the translation−rotation configuration space was sampled during the simulations. We employed the isothermal−isobaric ($NpT$) ensemble at $T$ = 298.15 K and $p$ = 1 atm, as well as the



https://doi.org/10.1021/acs.jpcb.1c10124
J. Phys. Chem. B 2022, 126, 2699−2714

standard numerical procedures described in the Supporting Information (SI).

The intermolecular interactions are described with a force field (FF) composed of Coulomb and LJ terms for the atomic pairs. Each atomic site is thus characterized by three parameters, namely the electric charge ($q_i$) and the LJ parameters associated with the potential depth ($\epsilon_i$) and the effective particle size ($\sigma_i$), where the subscript $i$ indicates the site. We used the extended simple point-charge (SPC/E)[54] parametrization for water−water interactions, which was also used to model the solvated electron.[49] The latter model is a suitable departing point because Pauli repulsion dominates the short-range Ps−water interactions.[28,41] The LJ parameters for the electron were optimized using the structural data obtained from electron paramagnetic resonance (EPR), as described by Ludwig et al.,[49] and could reproduce the maximum of the absorption spectrum of the solvated particle. It should be clear that the LJ contribution to the electron−water interaction is essentially the short-range repulsion, since the long-range interaction is largely dominated by the Coulombic charge−charge term. SPC/E neglects dispersion for the hydrogen atoms, considering the reduced electronic density arising from the polar OH bonds, such that only the Coulomb term accounts for the intermolecular H−H and O−H interatomic forces. For consistency, the electron−H interaction was described only with the Coulomb term.[49] Since the latter is zero for neutral atoms, our model only includes Ps−O interactions through the LJ term, in consistency with both the SPC/E and the solvated electron models.

The LJ potential for a Ps−O pair can be written as

$$U_{\mathrm{PsO}} = \frac{C_{12}^{\mathrm{PsO}}}{r^{12}} - \frac{C_{6}^{\mathrm{PsO}}}{r^{6}} \tag{1}$$

where $r$ is the interatomic distance, $C_6^{\mathrm{PsO}} = 4\epsilon\sigma^6$ and $C_{12}^{\mathrm{PsO}} = 4\epsilon\sigma^{12}$. The pair parameters are expressed in terms of the atomic ones as per the usual combination rule, $\epsilon = \sqrt{\epsilon_{\mathrm{Ps}}\epsilon_{\mathrm{O}}}$ and $\sigma = \sqrt{\sigma_{\mathrm{Ps}}\sigma_{\mathrm{O}}}$. We impose the repulsive term to be the same as in the solvated electron model, $C_{12}^{\mathrm{PsO}} = C_{12}^{e^-\mathrm{O}} = 6.44 \times 10^6$ Hartree $a_0^{12}$. The attractive term is obtained from a Slater−Kirkwood combination of atomic parameters[55]

$$C_6^{\mathrm{PsO}} = \frac{2C_6^{\mathrm{PsPs}}C_6^{\mathrm{OO}}}{\frac{\alpha_{\mathrm{Ps}}}{\alpha_{\mathrm{O}}}C_6^{\mathrm{OO}} + \frac{\alpha_{\mathrm{O}}}{\alpha_{\mathrm{Ps}}}C_6^{\mathrm{PsPs}}} \tag{2}$$

where $\alpha_{\mathrm{Ps}}$ and $\alpha_{\mathrm{O}}$ are the static polarizabilities of Ps and oxygen, respectively, while $C_6^{\mathrm{PsPs}}$ and $C_6^{\mathrm{OO}}$ are the dispersion coefficients for the Ps−Ps and O−O interactions. Essentially exact values can be obtained for the Ps atom,[41,56] $\alpha_{\mathrm{Ps}} = 36a_0^3$ and $C_6^{\mathrm{Ps-Ps}} = 207.97$ Hartree $a_0^6$, and the polarizability of the oxygen atom is also known,[57] $\alpha_{\mathrm{O}} = 5.41a_0^3$. The dispersion coefficient for a free oxygen pair is 15.6 Hartree $a_0^6$, although it ranges from 11.7 Hartree $a_0^6$ to 14.7 Hartree $a_0^6$ for bonded atoms.[55] We assumed $C_6^{\mathrm{OO}} = 12.6$ Hartree $a_0^6$, which is characteristic of a hydrogen-bonded water dimer, thus obtaining $C_6^{\mathrm{PsO}} = 45.5$ Hartree $a_0^6$.

In the MC simulations, we used the LJ parameters of the SPC/E model, which faithfully describes the thermodynamic properties of liquid water. The FF parameters for the Ps atom, $\epsilon_{\mathrm{Ps}} = 0.016$ kcal/mol and $\sigma_{\mathrm{Ps}} = 4.61$ Å, were chosen to ensure the $C_6^{\mathrm{PsO}}$ and $C_{12}^{\mathrm{PsO}}$ coefficients given above in combination with SPC/E. We also generated a more attractive Ps−O FF from the largest dispersion coefficient given by Tkatchenko and Scheffler[55] for bonded atoms, $C_6^{\mathrm{OO}} = 14.7$ Hartree $a_0^6$. As shown in the SI, several structural and thermodynamic properties of the Ps−water system remained essentially unchanged. This behavior could be anticipated since Ps is a hydrophobic species; that is, reasonable changes in the shallow LJ potential depth are immaterial. The neglect of dispersion forces between the Ps and the positively charged hydrogen atoms is further justified, since the additional FF parameters would not significantly improve the solvation model. The repulsive $C_{12}^{\mathrm{PsO}}$ coefficient emulates the Pauli repulsion for the solvated electron, and the latter effect also dominates Ps−water repulsion. The Ps model should therefore employ the same $C_{12}$ coefficient that describes the electron−water repulsive interaction. Most of our results were computed with the $C_{12}$ value consistent with the model proposed by Ludwig et al.,[49] as described above. This choice was very convenient since these authors employed the same QM/MM techniques implemented in the APMO framework. Nevertheless, the structural properties obtained by Ludwig et al., in particular the excluded volume and the coordination of the electron, are not in good agreement with several other theoretical accounts.[58,59] We performed additional calculations with a different $C_{12}$ coefficient for the electronic repulsive potential. It should be clear that we do not propose a new model for solvated electrons but rather explore the sensitivity of our Ps model with respect to the repulsive LJ coefficient.

**2.2. Quantum Calculations.** In our quantum calculations, the atomic nuclei were treated as fixed point charges under the Born−Oppenheimer approximation, while electrons and positrons were described as quantum particles with the multicomponent APMO approach[47] implemented in the LOWDIN package.[60] Wave functions were computed at the APMO Hartree−Fock (APMO/HF) level. Correlation energies, accounting for both electron−electron and electron−positron interactions, were obtained with the generalized APMO second-order propagator (APMO/P2) approach.[61]

Vertical detachment energies (VDEs) were obtained from Koopmans' theorem (KT) as the negative of the energies of electronic and positronic singly occupied molecular orbitals (SOMOs),

$$\mathrm{VDE}_{\mathrm{KT}}^{\alpha} = -\epsilon_p^{\alpha} \tag{3}$$

where $\epsilon_p^{\alpha}$ is the SOMO energy of $\alpha = e^-$ or $e^+$ for the $p$th orbital. In the framework of the multicomponent APMO propagator theory, KT energies can be improved by the inclusion of relaxation and correlation corrections via the self-energy term, $\sum_{pp}^{\alpha}(\omega_p^{\alpha})$, such that

$$\mathrm{VDE}_{\mathrm{P2}}^{\alpha} = -\omega_p^{\alpha} \tag{4}$$

where $\omega_p^{\alpha}$ is the optimized SOMO energy obtained by solving

$$\omega_p^{\alpha} = \epsilon_p^{\alpha} + \Sigma_{pp}^{\alpha}(\omega_p^{\alpha}) \tag{5}$$

iteratively, with

$$\Sigma_{pp}^{e^+}(\omega_p^{e^+}) = \mathcal{T}_{ORX}^{e^-} + \mathcal{T}_{PRM}^{e^+-e^-} \tag{6}$$



https://doi.org/10.1021/acs.jpcb.1c10124
J. Phys. Chem. B 2022, 126, 2699−2714

$$\Sigma_{pp}^{e^-}(\omega_p^{e^-}) = \Sigma_{pp}^{e^-e^-}(\omega_p^{e^-}) + \Sigma_{pp}^{e^-e^+}(\omega_p^{e^-}) \quad (7)$$

and

$$\Sigma_{pp}^{e^-}(\omega_p^{e^-}) = \mathcal{T}_{ORX}^{e^-} + \mathcal{T}_{ORX}^{e^+} + \mathcal{T}_{PRX}^{e^-e^+} + \mathcal{T}_{PRM}^{e^-e^-} + \mathcal{T}_{PRM}^{e^-e^+} \quad (8)$$

In the expressions above, $\mathcal{T}_{PRM}^{e^+e^-}$ and $\mathcal{T}_{PRM}^{e^-e^-}$ are the pair-removal correlation terms associated with the $e-p$ and $e-e$ correlations. The $\mathcal{T}_{ORX}^{e^+/e^-}$ terms describe positron/electron relaxation upon electron/positron detachment, and $\mathcal{T}_{PRX}^{e^-e^+}$ is the pair-relaxation term, which is only present if there is more than one occupied orbital.[61,62]

The classical MC simulations generate Ps−solvent configurations comprising 500 water molecules. It would not be possible to describe systems of that size employing the APMO methods described above. In most of the results presented in the next section, we consider a hybrid approach. The Ps atom and neighboring water molecules are treated quantum mechanically, although subjected to the electrostatic field of the far-lying water molecules. The field is generated by the same atomic point charges used in the FF, referred to as the electrostatic embedding. This hybrid QM/MM method was recently implemented in the LOWDIN code and is applied here for the first time. Finally, we also calculated the probability densities for the electronic and positronic orbitals with the Multiwfn software package,[63] using 500-point radial grids.

**2.3. Annihilation Rate.** The calculation of accurate annihilation rates from wave function or DFT methods is very challenging. Electron−positron pairs are strongly correlated systems requiring computationally intensive methods, so it is a common practice to resort to enhancement factors.[64,65] The present work is mainly focused on the QM/MM approach to solvated Ps atoms, paying special attention to the construction of the QM model, so we do not discuss enhancement factors or empirical corrections to the annihilation rates computed with APMO wave functions. We calculate two-photon annihilation rates to illustrate how the contributions from the direct and pick-off mechanisms can be easily obtained from the electronic and positronic molecular orbitals. Motivated by the potential relevance of the annihilation with core electrons to positron-based cancer treatments,[25] we also decompose the pick-off rates into the contributions from valence and core electrons.

The spin-averaged two-photon annihilation rate[66,67] ($\lambda$) for a solvated Ps atom can be expressed as

$$\lambda = \pi r_0^2 c \int \Psi^*(\vec{R}_e, \vec{r}_p)\delta(\vec{R}_e, \vec{r}_p)\Psi(\vec{R}_e, \vec{r}_p)d\vec{R}_e d\vec{r}_p \quad (9)$$

where $r_0$ is the classical electron radius, $c$ is the speed of light, and $\Psi$ is the APMO/HF wave function. The position of the positron is denoted as $\vec{r}_p$, while the electronic positions are collectively indicated as $\vec{R}_e$. It should be clear that the density operator is given by a sum over $N$ electrons, $\delta(\vec{R}_e, \vec{r}_p) \equiv \sum_{i=1}^{N}\delta(\vec{r}_i - \vec{r}_p)$, where $\vec{r}_i$ is the position of the $i$th electron. In view of the $\mathbf{r}_e = \mathbf{r}_p$ constraints imposed by the density operator for every electron−positron pair, the integral in eq 9 can be rewritten in terms of density overlaps involving the occupied electronic and positronic squared orbitals. In the unrestricted APMO/HF computations, the densities are converged without imposing spin states for the positron and the unpaired electron, so the rate can be written as

$$\lambda = \pi r_0^2 c\left(S_N + \sum_{i=1}^{N_\alpha} S_i^\alpha + \sum_{j=1}^{N_\beta} S_j^\beta\right). \quad (10)$$

We consider Ps-$(H_2O)_n$ aggregates described quantum mechanically with $N = (N_\alpha + N_\beta + 1)$ electrons, where $N_\alpha$ and $N_\beta$ are the numbers of $\alpha$- and $\beta$-spin electrons in the neutral water cluster (closed shell, $N_\alpha = N_\beta$). $S_i^\alpha = \int d\mathbf{r}\,|\phi_\alpha^i(\mathbf{r})|^2|\varphi(\mathbf{r})|^2$ is the overlap between the density of the $i$th electronic orbital with $\alpha$ spin ($\phi_\alpha^i$) and the density of the occupied positronic orbital ($\varphi$). The $\beta$-spin density overlaps, $S_i^\beta$, are defined likewise. The first term in parentheses ($S_N$) describes the direct annihilation rate, $\lambda_{Ps}$. For the fully antisymmetric electronic state, it is defined as the contribution from the spin−orbital describing the unpaired electron, denoted as $N$. The other terms ($S_i^\alpha$ and $S_j^\beta$) account for the pick-off rate, $\lambda_{po}$. Although not indicated explicitly, the contribution from the core and valence electrons to $\lambda_{po}$ can be calculated by classifying the electronic orbitals accordingly. The annihilation lifetimes ($\tau = 1/\lambda$) and the radial pick-off annihilation densities, corresponding to the integrands of the overlaps as functions of the radial coordinate, were calculated with Becke's multicenter algorithm[68] implemented in the Multiwfn package. The results obtained with a three-dimensional grid with 75 radial points and 434 angular points did not significantly differ from those computed with a denser grid having 250 radial and 5810 angular points.

## 3. RESULTS AND DISCUSSION

In sections 3.1−3.3, we discuss the results obtained with the LJ parameters for the Ps−O interaction given in section 2.1, based on the hydrated electron model reported by Ludwig et al.[49] The reduced cavity model, which employed a modified set of LJ parameters, is discussed in section 3.4.

**3.1. Classical Results.** The radial distribution function (RDF) for Ps−oxygen pairs, shown in Figure 1 (red line), provides information on the solvent structure around the solute. The first solvation shell is defined by the RDF

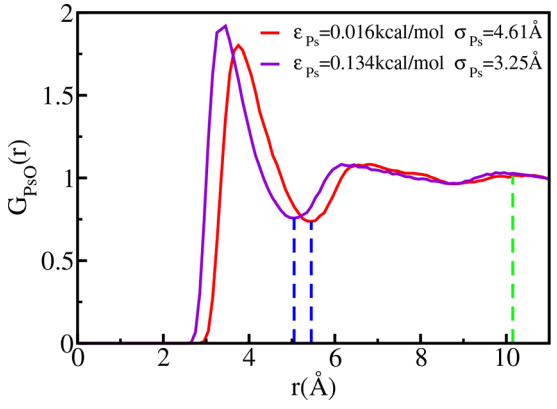


**Figure 1.** Radial distribution function for Ps−oxygen pairs. The hydrated Ps model based on the parametrization of ref 49 is given by the solid red line, while the solid purple line was computed with a different set of LJ parameters. The dashed lines define the first solvation shell (blue) and bulk limit (green) with $G_{PsO}(r) = 1$.



https://doi.org/10.1021/acs.jpcb.1c10124
J. Phys. Chem. B 2022, 126, 2699−2714

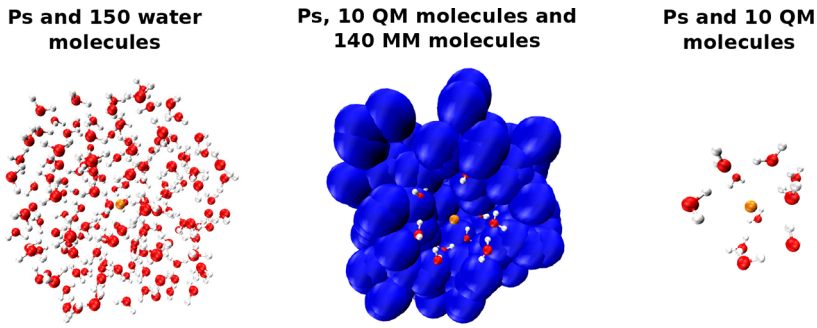


**Figure 2.** Structure of Ps−water configuration A (see text). The solvation shells up to the bulk limit comprise 150 water molecules (left), with the oxygen, hydrogen, and Ps atoms represented in red, white, and yellow, respectively. The QM/MM model (center) comprises ten water molecules in the QM region and 140 in the MM region. The QM molecules are represented by balls and sticks, while the MM ones are represented by large blue spheres. The isolated cluster is formed only by the QM region (right), without electrostatic embedding.

minimum at 5.45 Å, indicated by the dashed blue line, and displays a maximum around 3.75 Å. A second solvation shell is also noticeable, and the bulk density, corresponding to $G_{PsO}(r) = 1$, is observed beyond 10.15 Å, as indicated by the dashed green line. Integration of the RDF points out 22 water molecules in the first shell ($r \leq 5.45$ Å) and 150 molecules up to the bulk limit ($r \leq 10.15$ Å). The RDF also points out a solute cavity, with a radius of ≈3.0 Å, in consistency with the hydrophobic character of Ps. This cavity radius is also close to the empirical estimate obtained for the bubble model, $R = 3.2$ Å.[39]

The Ps hydration free energy, $\Delta G_{hyd}$, was calculated with the free energy perturbation (FEP) method[69,70] using the procedure as performed before.[71] The Ps−water interaction potential was gradually turned off by decreasing the LJ parameters stepwise, as described in the SI, such that $\Delta G_{hyd} = 5.58 \pm 0.32$ kcal/mol was obtained as minus the free energy for Ps disappearance in solution. The positive value indicates a nonspontaneous process, and the solvation free energy for Ps in water is comparable in magnitude to those reported for neon (2.48 kcal/mol) and xenon (1.45 kcal/mol), which are examples of hydrophobic solutes forming clathrate structures.[72] The Ps solvation energy, $\Delta E_{hyd}$, was also estimated as the energy difference between the noninteracting Ps−water system and the solvated Ps counterpart,

$$\Delta E_{hyd} = E_{solv} - E_{free} = (E_{Psw} + E_{ww}^{Ps}) - (E_{ww}^{bulk}) \quad (11)$$

Since the classical simulations disregard the internal structures of atoms and molecules, the energy of the noninteracting system ($E_{free}$) only considers bulk water−water intermolecular interactions ($E_{ww}^{bulk}$), while Ps−water ($E_{Psw}$) and water−water interactions in the presence of Ps ($E_{ww}^{Ps}$) are considered in the solvated system ($E_{solv}$). As described in the SI, all terms in eq 11 are averaged over the MC configurations computed for the water molecules lying within the cutoff radius employed in the simulations using the procedure as performed before.[73] The solvation energy is more conveniently expressed in terms of the solvent relaxation energy,

$$\Delta E_{hyd} = E_{Psw} + E_{rlx} \quad (12)$$

where $E_{rlx} = (E_{ww}^{Ps} - E_{ww}^{bulk})$. The calculated solvation energy, $\Delta E_{hyd} = -11.25 \pm 1.32$ kcal/mol, is largely dominated by the relaxation contribution, $E_{rlx} = -11.24 \pm 1.30$ kcal/mol, since the average interaction of the hydrophobic Ps particle with the solvent is weak, $E_{Psw} = -0.01 \pm 0.02$ kcal/mol. From basic thermodynamics principles, the entropy change associated with Ps solvation can be expressed as

$$\Delta S_{hyd} = \frac{1}{T}(\Delta E_{hyd} - \Delta G_{hyd} + p\Delta V) \quad (13)$$

where $p\Delta V$ is the volume change associated with Ps solvation (see the SI for details). We obtained $\Delta S_{hyd} = -244 \pm 23$ J/mol·K from the energy estimates given above and the $p\Delta V$ contribution. The negative entropy change arises from the breaking of the hydrogen bonds to form the solute cavity. The water molecules in the first solvation shell become oriented such that their hydrogen bonds are tangent to the cavity surface and their mobility is reduced. A similar decrease in the rotational and translational entropies of water molecules was observed by Halselmeier et al. in the solvation of xenon atoms.[74] This corroborates the parallel between the solvation of noble gases and Ps, since the hydrated exotic particle also forms a clathrate structure.

**3.2. Cluster Models.** The statistical correlation among the MC configurations was characterized with a standard procedure based on the enthalpy autocorrelation function.[75,76] Uncorrelated configurations were found to be separated by ≈$1.2 \times 10^6$ steps, such that 80 uncorrelated configurations were selected out of $2 \times 10^5$ ones generated along the simulations. While the statistically uncorrelated configurations play a crucial role in the model, as they allow for estimates of thermodynamically averaged quantum properties, caution must be taken to keep the numerical effort manageable. Crucial variables are the level of electron−positron correlation in the APMO calculations, the basis set size, and the number of QM molecules in the Ps−water clusters. One should bear in mind that considering Ps−water configurations with 500 solvent molecules would be impractical. The combination of QM water molecules with far-lying MM ones (electrostatic embedding) can provide a compromise between accuracy and effort.

The convergence of the quantum properties was studied with respect to the basis set size and expansion centers. To this end, we considered the total energies of the Ps−water clusters, the radial probability densities, and the electronic and positronic vertical VDEs. The latter are given by minus the energies of the unpaired molecular orbitals, thus corresponding to electronic and positronic ionization potentials. Preliminary studies indicated that a QM region comprising ten water molecules was reasonable to assess the basis set quality. As shown in Figure 2, that choice corresponds to the average


https://doi.org/10.1021/acs.jpcb.1c10124
J. Phys. Chem. B 2022, 126, 2699−2714

number of first neighbors and can be viewed as the coordination number of the Ps atom. We performed calculations for three representative uncorrelated configurations labeled A, B, and C, selected on the basis of different solvent molecule distributions around the solute. The first is shown in Figure 2, and the other ones are shown in the SI. While the first solvation shell is composed of 22 water molecules, as explained in section 3.1, the smaller QM clusters are convenient to reduce the numerical effort.

We performed APMO/HF calculations for the isolated clusters (QM region only) and for the clusters surrounded by the electrostatic embedding (QM and MM regions). In the latter case, 140 water molecules were described with effective atomic charges, such that the sum of water molecules in the QM and MM regions accounts for the first and second solvation shells (see section 3.1).

*3.2.1. Basis Sets.* The numerical burden can be significantly affected by the choice of basis set. In addition to the Gaussian basis, one should consider the number of expansion centers, especially for the positronic wave function. We explored three different schemes: (I) All atomic centers in the QM region, namely the oxygen and hydrogen atoms in the water molecules described explicitly, were used to expand the electronic wave function, although only the QM oxygen centers were used to expand the positronic wave function. This procedure avoids too large basis sets and can be justified by the repulsive interaction between the positron and the positively charged hydrogen atoms. (II) The positronic wave function was expanded with a single ghost center placed at the position of the Ps atom in the MC configuration, i.e., inside the solute cavity. The electronic wave function used in the previous scheme was also augmented with atomic orbitals (AOs) on the same ghost center. (III) All QM centers described above were combined such that the positronic wave function was expanded on both the oxygen and ghost centers, while the electronic wave function was the same as in scheme II. In schemes II and III, standard hydrogenic basis sets were added at the ghost center for both the electronic and positronic wave functions.

The three schemes outlined above were tested with several basis sets for the A, B, and C configurations. In all cases, we also performed calculations with and without electrostatic embedding. While most of the results are presented in the SI, the take-home lesson can be learned from Table 1, which shows the total APMO/HF energies obtained for configuration A with the 6-31G++(d,p) basis set. In general, the energy improvement with respect to the basis set size is very slow in scheme I. The energies obtained with the APMO/HF/6-31G++(d,p) method for configuration A are significantly lower for scheme II (322 AOs) compared to scheme I (500 AOs), despite the larger number of AOs in the latter. The energy differences are around 0.030 and 0.050 hartree for the isolated and embedded QM clusters, respectively.

The energies computed with scheme III (512 AOs) are even lower, as expected, although the improvement with respect to scheme II is relatively small in view of the basis set sizes. The energy differences were 0.018 and 0.016 hartree for the isolated and embedded systems, respectively. The use of scheme II can be viewed as the best compromise between numerical effort and accuracy, and it could be further improved by optimizing the basis sets centered inside the solute cavity.

The molecular orbital (MO) amplitudes and the radial probability densities provide further insight into the basis set quality. Figure 3 shows the radial probability densities (RPDs) for the unpaired molecular orbitals obtained with the APMO/HF/6-31G++(d,p) method for configuration A (results for configurations B and C are shown in the SI). Even though we performed unrestricted HF calculations, we henceforth refer to those orbitals as singly occupied molecular orbitals (SOMOs), and their amplitudes are shown in Figure 4. Both the excess electron and the positron tend to delocalize over the cluster surface when scheme I is used. The densities of both particles are shifted inward in the embedded cluster, but most of the probabilities still lie outside the solute cavity ($r$ > 3.0 Å). Despite the diffuse basis set employed in the calculations, the RPDs are strikingly different in scheme II. Most of the electronic and positronic SOMO densities become localized inside the solute cavity. Apart from minor outward shifts, the SOMO densities obtained with scheme III are similar to those calculated with scheme II. In both schemes, the electrostatic embedding has mild effects on the RPDs, although the electronic SOMO is somewhat more localized inside the cavity in the embedded cluster.

The excess charge in water cluster anions can be either localized "inside" the cluster volume or delocalized over the surface, depending on the cluster size and other aspects.[77,78] Positron attachment to neutral glycine−water clusters also gives rise to far-lying positronic densities localized around the negative end of the dipole moment of the cluster.[79] One could thus argue if the addition of AOs inside the solute cavity could artificially enforce charge localization. We actually believe this is not the case. The comparison of the variational APMO/HF energies for schemes I and II points out that better (lower) energies are obtained with much smaller basis sets in the case when the ghost center is used. The combination of all expansion centers (scheme III) also gives rise to even lower energies and localized SOMO densities, similar to those obtained with scheme II. The results suggest that scheme I would require significantly larger basis sets located on the relatively far-lying atomic centers to properly describe the electronic and positronic densities inside the cavity. We thus consider the densities obtained with scheme I to be artificially produced by inadequate basis sets.

We further explored scheme II with larger basis sets, although only considering the embedded cluster obtained from configuration A. The RPDs calculated for the electronic SOMO are shown in Figure 5. In the first set of calculations, we used the 6-31G+(d,p), 6-31G++(d,p), 6-311G++(d,p), and aug-cc-pVDZ basis sets for the electrons and the positron. As long as the basis set is sufficiently diffuse, which is the case for the 6-31G++(d,p), 6-311G++(d,p), and aug-cc-pVDZ calculations, the positronic densities are similar. We also considered

**Table 1. Total Energies (in Hartree) Obtained with the APMO/HF/6-31G++(d,p) Method for the Configuration A[a]**

| | total energy | | |
|---|---|---|---|
| expansion centers | isolated | embedded | $N_{AO}$ |
| oxygen | −760.3196 | −807.7798 | 500 |
| ghost | −760.3498 | −807.8300 | 322 |
| oxygen and ghost | −760.3676 | −807.8463 | 512 |

[a]The calculations were performed for the isolated and embedded clusters employing schemes I (oxygen), II (ghost), and III (oxygen and ghost) for the expansion centers (see text). The number of atomic orbitals ($N_{AO}$) is also indicated.



https://doi.org/10.1021/acs.jpcb.1c10124
J. Phys. Chem. B 2022, 126, 2699−2714

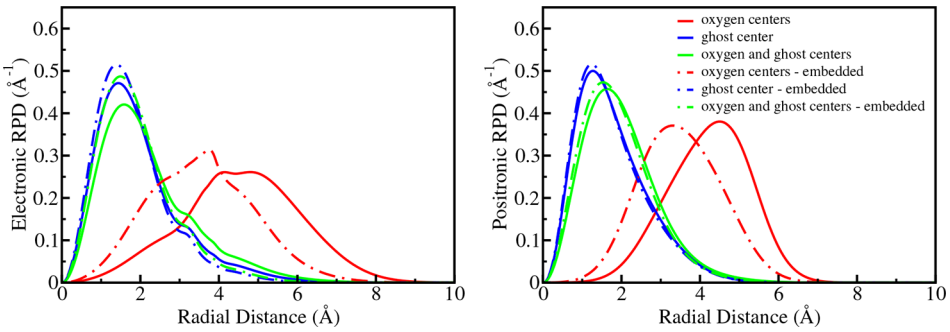


**Figure 3.** Radial probability densities for the electronic (left) and positronic (right) SOMO orbitals obtained for configuration A with the APMO/HF/6-31G++(d,p) method. The calculations were performed for the isolated (solid lines) and embedded (dot−dashed lines) QM clusters. Schemes I (oxygen centers), II (ghost center), and III (oxygen and ghost centers) for the basis set expansion were also considered (see text).

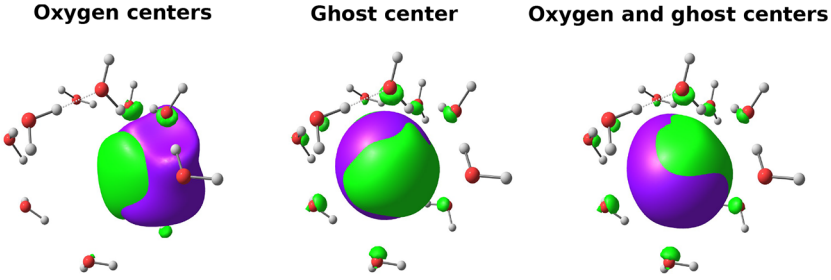


**Figure 4.** Isosurfaces of the electronic (green) and positronic (purple) SOMO orbitals obtained for configuration A with the APMO/HF/6-31G++(d,p) method. The calculations were performed for the embedded QM clusters. Schemes I (oxygen centers), II (ghost center), and III (oxygen and ghost centers) for the basis set expansion were also considered (see text). The isovalue 0.03 au was used in all cases.

different basis sets for the atomic and ghost centers, denoted as 6-31G+(d,p)/aug-cc-pVXZ, with X = D, T, and Q. The 6-31G+(d,p) basis set was always used on the atomic centers, while the augmented correlation-consistent (aug-cc) basis sets expanded the ghost center. Once more, no significant change in the RPDs was observed, pointing out that the combination of scheme II with the 6-31G+(d,p)/aug-cc-pVDZ basis set would provide a suitable balance between accuracy and effort.

*3.2.2. Detachment Energies.* While the total energy is useful to access the basis set quality in variational APMO/HF calculations, it is not observed in experiments. The VDE, on the other hand, is often used to characterize electron−water clusters[78,80] and could also be useful for positrons, at least in principle. The electronic and positronic VDEs, estimated from Koopmans' theorem applied to the APMO/HF SOMOs, are shown in Table 2. Once more, we consider several basis sets for configuration A (see the SI for configurations B and C) and also different schemes for the basis set expansion centers. As expected, the results obtained with scheme I are discrepant, so we concentrate the discussion on schemes II and III. For these schemes, the electronic VDEs computed with the 6-31G+(d,p) basis set are in poor agreement with the other estimates. In general, the difference between the VDEs obtained for the isolated and embedded clusters is also underestimated compared to those computed larger basis sets. Focusing on the larger and more diffuse basis sets, 6-31G++(d,p) to aug-cc-pVDZ, it is clear that the interaction with the electrostatic embedding stabilizes the SOMOs, especially the positronic orbital (≈0.2 eV and ≈0.4 eV for schemes II and III, respectively). Also, for the larger basis sets, scheme III typically gives rise to smaller VDEs compared to scheme II, with more significant discrepancies for the electronic orbitals. For the embedded QM cluster, the 6-311G++(d,p) and aug-cc-pVDZ basis sets predict essentially the same positronic VDEs, although discrepancies around 0.4 to 0.5 eV (≈10%) are found for the electronic detachment energy.

Since the electronic basis sets are the same in schemes II and III, the VDE discrepancies for the electronic SOMO actually arise from the localization of the positron density. In other words, the slightly more compact positronic wave function (scheme II) attracts the excess negative charge more effectively, thus shifting the electronic density from the outer region of the QM cluster to the solute cavity. Inspection of the RPDs in Figure 3 further supports the argument. The positron density is shifted inward in scheme II, with respect to scheme III, and the corresponding electron density peak becomes higher and slightly shifted inward. The fact that the electronic VDE is more significantly affected by the change in the positron basis is counterintuitive, but the accumulation of electronic density in the cavity leads to stabilization by two effects, namely the more effective attraction to the positron density and the smaller electron repulsion. Finally, we computed the VDEs employing scheme II and the 6-31G+(d,p)/aug-cc-pVXZ basis sets described above, as shown in Table 3. The electronic VDE is barely affected by the basis set placed on the ghost center or the embedding ($10^{-2}$ eV variations), although still overestimated, by about 10%, compared to the result obtained with scheme III employing the larger basis sets. The positronic VDE is more sensitive to the basis set and embedding, with variations around $10^{-1}$ eV. Unlike the total energy, the VDEs do not show a clear trend with respect to the basis set size, and the discrepancies between schemes II and III, although not large, are persistent. Comparing the estimates obtained for the embedded cluster with scheme III and the 6-311G++(d,p) basis set (Table 2) with those computed with scheme II and the 6-31G+(d,p)/


https://doi.org/10.1021/acs.jpcb.1c10124
J. Phys. Chem. B 2022, 126, 2699−2714

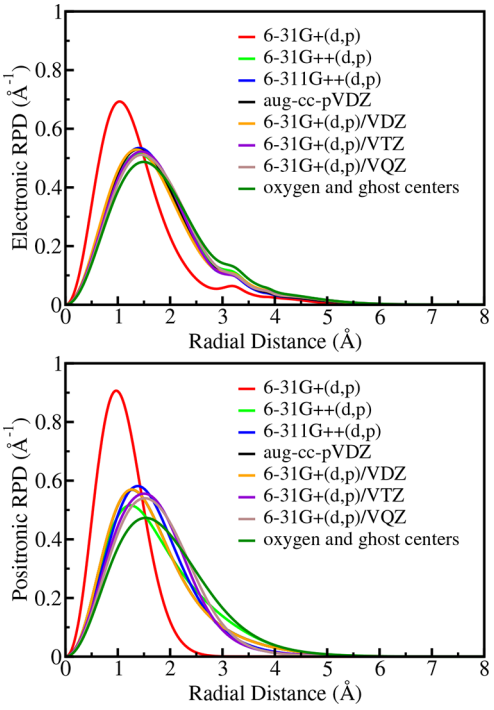


**Figure 5.** Radial probability densities for the electronic (upper panel) and positronic (lower panel) SOMO orbitals obtained for configuration A with the APMO/HF method and scheme II for the expansion centers (see text). The 6-31G+(d,p), 6-31G++(d,p), 6-311G++(d,p), and aug-cc-pVDZ basis sets were used for the electronic and positronic wave functions. The electronic 6-31G+(d,p) basis set in the atomic centers was also combined with aug-cc-pVXZ sets in the ghost center, where X = D, T, and Q. The basis set combinations are indicated as 6-31G+(d,p)/VXZ. The result obtained with scheme III and the 6-31G++(d,p) basis set is also shown for comparison (oxygen and ghost centers).

VQZ basis set (Table 3), we find better agreement for the positronic VDE (0.06 eV) than for the electronic counterpart (0.37 eV). The discrepancies between the VDE estimates computed with schemes II and III can be view as tolerable considering the significant difference in the basis set sizes, especially for the more sophisticated model with a larger QM region and the inclusion of electronic and positronic correlation effects.

*3.2.3. Annihilation Lifetimes.* Electron−positron pairs form strongly correlated Fermion systems. An accurate description of the correlation energies and annihilation rates requires the inclusion of high-order terms in the many-body perturbation expansion.[81] Since the use of accurate, although computationally intensive methods would be unfeasible for systems comprising tens of atoms, the quantitative description of the pair annihilation rates would require empirical corrections, such as enhancement factors.[64,65] While the development of these corrections is beyond the scope of the present work, we present two-photon annihilation lifetimes (reciprocal annihilation rates) obtained from the APMO/HF molecular orbitals, as described in section 2.3. The direct (intrinsic) lifetimes, $\tau_{Ps}$, are computed with the electronic SOMO, while the pick-off counterparts, $\tau_{po}$, are computed with paired orbitals. The core contribution to the latter lifetimes, $\tau_{co}$, is simply obtained by classifying the electronic orbitals as core or valence ones. The direct annihilation rate is the major component of PET signals, pick-off annihilation encodes information about the medium in PALS, and core annihilation could be relevant to positron-based cancer therapy.

The lifetimes obtained for configuration A with the different expansion schemes and several basis sets are shown in Table 4 (see the SI for configurations B and C). The pick-off lifetimes computed with scheme I are fairly close to the room-temperature experimental result, $\tau_{po}$ = 1.85 ns.[39] Scheme I provides a poor description of the solvated Ps, as discussed above, and the HF wave functions are expected to significantly overestimate the annihilation lifetimes (underestimate the annihilation rates).[82] The reasonable agreement between the pick-off rates calculated with scheme I and the experimental data is accidental. The $\tau_{po}$ lifetimes are decreased by the artificial displacement of the Ps density from the solute cavity into the region with high electronic density (see Figures 4 and

**Table 3. Electronic ($e^-$) and Positronic ($e^+$) VDEs (in eV) Estimated with Koopmans' Theorem for Configuration A[a]**

| | isolated | embedded | basis set |
|---|---|---|---|
| $e^-$ VDE | 4.97 | 4.99 | 6-31G+(d,p)/VDZ |
| | 4.96 | 4.96 | 6-31G+(d,p)/VTZ |
| | 4.96 | 4.95 | 6-31G+(d,p)/VQZ |
| $e^+$ VDE | 4.45 | 4.56 | 6-31G+(d,p)/VDZ |
| | 4.56 | 4.72 | 6-31G+(d,p)/VTZ |
| | 4.56 | 4.75 | 6-31G+(d,p)/VQZ |

[a]The calculations were performed for the isolated and embedded clusters using different basis sets and scheme II for the expansion centers (see text). The 6-31G+(d,p) basis set was used in the atomic centers, and aug-cc-pVXZ was used in the ghost center, where X = D, T, and Q. The basis set combinations are indicated as 6-31G+(d,p)/VXZ.

**Table 2. Electronic ($e^-$) and Positronic ($e^+$) VDEs (in eV) Estimated with Koopmans' Theorem for Configuration A[a]**

| | oxygen centers | | ghost center | | oxygen and ghost centers | | |
|---|---|---|---|---|---|---|---|
| | isolated | embedded | isolated | embedded | isolated | embedded | basis set |
| $e^-$ VDE | 2.38 | 2.67 | 6.26 | 6.32 | 4.53 | 4.66 | 6-31G+(d,p) |
| | 2.97 | 3.74 | 4.73 | 4.81 | 4.42 | 4.53 | 6-31G++(d,p) |
| | 3.03 | 3.18 | 4.93 | 4.99 | 4.46 | 4.58 | 6-311G++(d,p) |
| | 3.01 | 3.13 | 4.96 | 5.02 | 4.42 | 4.50 | aug-cc-pVDZ |
| $e^+$ VDE | 3.89 | 3.63 | 4.27 | 4.25 | 4.53 | 4.57 | 6-31G+(d,p) |
| | 3.10 | 2.54 | 4.17 | 4.40 | 4.29 | 4.63 | 6-31G++(d,p) |
| | 3.21 | 3.01 | 4.51 | 4.69 | 4.34 | 4.69 | 6-311G++(d,p) |
| | 3.68 | 3.42 | 4.42 | 4.58 | 4.24 | 4.62 | aug-cc-pVDZ |

[a]The calculations were performed for the isolated and embedded clusters using different basis sets and schemes I (oxygen centers), II (ghost center), and III (oxygen and ghost centers) for the expansion centers (see text).



https://doi.org/10.1021/acs.jpcb.1c10124
J. Phys. Chem. B 2022, 126, 2699−2714

Table 4. Annihilation Lifetimes (in Nanoseconds) Calculated with the APMO/HF Method for Configuration A with Schemes I (Oxygen Centers), II (Ghost Center), and III (Oxygen and Ghost Centers) Described in the Text[a]

| | oxygen centers | | ghost center | | oxygen and ghost centers | | |
|---|---|---|---|---|---|---|---|
| | isolated | embedded | isolated | embedded | isolated | embedded | basis set |
| $\tau_{Ps}$ | 12.73 | 10.31 | 2.49 | 2.47 | 5.11 | 4.79 | 6-31G+(d,p) |
| | 25.24 | 15.15 | 7.89 | 6.88 | 11.07 | 8.79 | 6-31G++(d,p) |
| | 22.64 | 15.30 | 7.20 | 6.53 | 10.64 | 8.47 | 6-311G++(d,p) |
| | 21.94 | 16.37 | 6.86 | 6.25 | 11.42 | 9.06 | aug-cc-pVDZ |
| $\tau_{po}$ | 2.20 | 2.57 | 97.13 | 98.11 | 7.98 | 8.72 | 6-31G+(d,p) |
| | 2.13 | 2.76 | 2.76 | 2.95 | 8.53 | 9.61 | 6-31G++(d,p) |
| | 2.33 | 2.79 | 4.59 | 4.89 | 8.68 | 9.74 | 6-311G++(d,p) |
| | 2.78 | 3.26 | 3.71 | 3.95 | 8.83 | 9.83 | aug-cc-pVDZ |
| $\tau_{co}$ | 176.3 | 101.5 | 40891 | 40911 | 328.0 | 329.5 | 6-31G+(d,p) |
| | 203.5 | 117.5 | 16.37 | 17.59 | 1255 | 1642 | 6-31G++(d,p) |
| | 425.4 | 586.5 | 32.36 | 35.12 | 2543 | 3049 | 6-311G++(d,p) |
| | 137.2 | 100.2 | 22.39 | 24.09 | 2384 | 2200 | aug-cc-pVDZ |

[a]The calculations were performed for the isolated and embedded QM clusters with different basis sets.

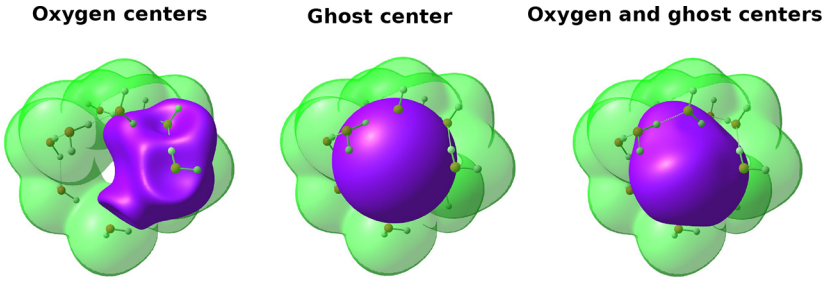


**Figure 6.** Isosurfaces of the pick-off electronic density (green) and positronic density (purple) obtained for embedded configuration A with the APMO/HF/6-31G++(d,p) method. Schemes I (oxygen centers), II (ghost center), and III (ghost and oxygen centers) for the basis set expansion were also considered (see text). The isovalue 0.0001 au was used in all cases.

6), thus enhancing annihilation. Those displaced Ps densities also increase the $\tau_{co}$ lifetimes with respect to scheme III. In this case, the overlaps of the positronic orbital with the core orbitals of the far-lying water molecules become vanishingly small.

As could be anticipated from the VDE results, the lifetimes calculated with the 6-31G+(d,p) basis set are generally in poor agreement with those computed with the more diffuse basis sets. The discrepancy is huge for $\tau_{po}$ and $\tau_{co}$ computed with scheme II, compared to scheme III. The short-ranged basis, along with the single-center expansion of the positronic orbital, unsuitably reduces the overlap of the positronic orbital with the doubly occupied electronic orbitals localized on the water molecules. In the following, we consider the lifetimes calculated with schemes II and III and the larger basis sets, i.e., all but 6-31G+(d,p). Since the annihilation lifetimes are mildly affected by the electrostatic embedding, we also concentrate the discussion on the basis sets and expansion centers.

The direct annihilation lifetimes predicted by scheme II are shorter by 20% to 30% in comparison with scheme III. The annihilation enhancement is consistent with the more localized SOMOs in scheme II, as discussed above, although it can be considered an artifact of the basis set expansion. While the estimates obtained with the 6-31G+(d,p)/aug-cc-pVXZ basis sets (Table 5) are somewhat closer to those computed with scheme III (Table 4), discrepancies persist. The disagreement between schemes II and III is significantly larger for the pick-off lifetimes. The $\tau_{po}$ values computed with scheme II are smaller in comparison with scheme III by a factor of 2 to 3,

Table 5. Annihilation Lifetimes (in Nanoseconds) for Configuration A Calculated with the APMO/HF Method[a]

| | isolated | embedded | basis set |
|---|---|---|---|
| $\tau_{Ps}$ | 6.69 | 6.22 | 6-31G+(d,p)/VDZ |
| | 7.27 | 6.70 | 6-31G+(d,p)/VTZ |
| | 7.46 | 6.87 | 6-31G+(d,p)/VQZ |
| $\tau_{po}$ | 3.79 | 3.96 | 6-31G+(d,p)/VDZ |
| | 5.64 | 5.94 | 6-31G+(d,p)/VTZ |
| | 5.83 | 6.14 | 6-31G+(d,p)/VQZ |
| $\tau_{co}$ | 22.98 | 24.22 | 6-31G+(d,p)/VDZ |
| | 43.61 | 46.10 | 6-31G+(d,p)/VTZ |
| | 47.75 | 50.41 | 6-31G+(d,p)/VQZ |

[a]Scheme II for the expansion centers was employed with different basis sets (see text). The 6-31G+(d,p) basis set was used in the atomic centers, while aug-cc-pVXZ was used in the ghost center, where X = D, T, and Q. The basis set combinations are indicated as 6-31G+(d,p)/VXZ. The lifetimes were decomposed into direct ($\tau_{Ps}$), pick-off ($\tau_{po}$), and core ($\tau_{co}$) terms for the isolated and embedded clusters.

and also more sensitive to the choice of basis set (Table 4). Once more, the discrepancies are mitigated by the 6-31G+(d,p)/aug-cc-pVXZ basis sets (Table 5), especially the VTZ and VQZ ones, but not removed.

The shorter pick-off lifetimes predicted by scheme II may seem counterintuitive at first glance. The single-center expansion of the positronic orbital favors the localization inside the solute cavity and would thus disfavor the overlap with the electronic orbitals localized on the water molecules. In


https://doi.org/10.1021/acs.jpcb.1c10124
J. Phys. Chem. B 2022, 126, 2699−2714

Figure 6 we show isosurfaces of the positronic density along with the corresponding pick-off electronic densities, which were obtained from the doubly occupied orbitals (excluding the electronic SOMO). For the three configurations (B and C are shown in the SI), scheme II gives rise to nearly spherically symmetric positronic densities, while the additional expansion centers in scheme III produce distorted densities. Since the $\tau_{po}$ lifetimes obtained from the latter positronic densities are shorter, we conclude that the more flexible positronic basis lowers the overlap with the pick-off electronic density. The APMO/HF wave functions minimize the total energy, so the deformation of the positronic orbital should alleviate the repulsive interaction with the atomic nuclei of the surrounding water molecules. This argument is consistent with the VDE results as scheme III predicts larger detachment energies (see Table 2 and the SI), although the discrepancies with respect to scheme II are more significant for the pick-off lifetimes. The considerably longer core annihilation lifetimes predicted by scheme III (Table 4) further suggest that the distortions of the positronic density avoid the vicinity of the nuclei.

The contributions from core orbitals to the pick-off lifetimes are particularly sensitive to the choice of expansion centers, as indicated by the strikingly large discrepancies between the $\tau_{co}$ values computed with schemes II and III, around 2 orders of magnitude. As far as the pick-off lifetimes are concerned, those huge differences are not very important because the core contribution does not exceed ≈15% in scheme II, being much smaller in scheme III. Nevertheless, the Auger decays initiated by core annihilation events enhance the probability of lethal DNA damage, which would make positron-based cancer treatments more efficient than the electron-based counterparts.[25] Our results point out that core annihilation lifetimes are even more challenging to theory than the pick-off ones.

Finally, we explored the radial pick-off overlap, which corresponds to the integrand of $\left(\sum_i S_i^{\alpha} + \sum_j S_j^{\beta}\right)$ in eq 10 as a function of the radial coordinate (integrated over all directions). These overlaps are shown in Figure 7 for configuration A and the 6-311G++(d,p) basis set (see the SI for configurations B and C). The pick-off overlaps obtained from scheme II have sharp peaks around 3.4 Å, thus lying close to the first maximum of the Ps−oxygen radial distribution function (Figure 1). Scheme III displays a lower peak, which is also shifted inward to 3.0 Å. This result provides further evidence that the multicenter expansion lowers the superposition of the positronic and pick-off electronic densities. The pick-off overlap densities obtained from Schemes II and III spread over ≈2.5 Å and ≈2.0 Å, respectively. These values can be related to the pick-off penetration thickness in the bubble model. The typical value $\delta$ = 1.66 Å[28] is comparable to the widths of the pick-off densities.

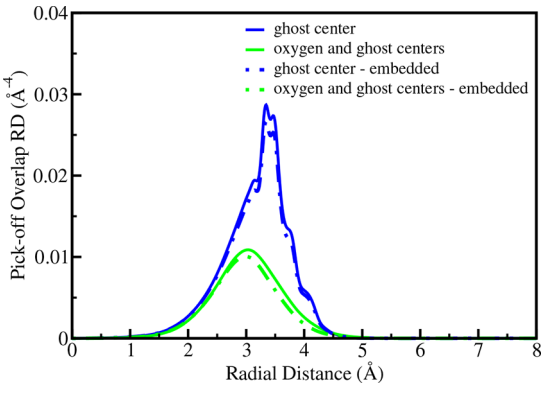


**Figure 7.** Radial pick-off overlap obtained for configuration A with the APMO/HF/6-311G++(d,p) method. The calculations were performed for the isolated and embedded QM clusters. Schemes II (ghost center) and III (oxygen and ghost centers) for the basis set expansion were also considered (see text).

**3.3. Bulk Model.** While the QM/MM models for small water clusters were useful for the numerical tests discussed in the previous sections, we further considered a larger model. We included 22 water molecules in the QM region, corresponding to the first solvation shell, in addition to 128 solvent molecules described as point charges. This procedure is often adequate to account for the absorption spectra of solvated molecules, so it should also account for the bulk properties of the solvated Ps atoms.

Although the results obtained with schemes II and III for the basis set expansions were not always in good agreement, especially for the annihilation lifetimes, the computations for the bulk model employed scheme II with the 6-31G+(d,p)/aug-cc-pVTZ basis set. It should be clear that the computational effort is increased by the larger number of molecules in the QM regions, the inclusion of correlation effects through the APMO/P2 method, and the statistical analysis. The latter was carried out with 80 uncorrelated configurations.

Before we consider the thermodynamical averages, it is interesting to compare the VDEs computed with the cluster and bulk models, respectively comprising 10 and 22 solvent molecules in the QM region. To this end, we resort to the A, B, and C configurations and the 6-31G+(d,p)/aug-cc-pVTZ basis set with scheme II for the expansion centers. The electronic VDEs obtained with the bulk (cluster) model were 4.94 eV (4.96 eV) for configuration A, 4.11 eV (3.86 eV) for configuration B, and 5.07 eV (4.81 eV) for configuration C. The positronic VDE estimates were 4.87 eV (4.72 eV), 5.65 eV (5.71 eV), and 4.89 eV (4.75 eV) for configurations A, B, and C, respectively. Comparing the models, the VDE deviations are not large, around and below 5%. These discrepancies are also considerably smaller than the differences among the estimates obtained for the A, B, and C configurations with the same model, suggesting that embedded small clusters may serve as reasonable models for VDE calculations.

The VDE estimates computed with the APMO/HF and APMO/P2 methods for the bulk model are presented in Table 6. The mean values and mean errors, corresponding to the standard error of the mean, were obtained from the set of 80 uncorrelated Ps−solvent configurations. The HF-level positronic VDE, 5.33 ± 0.04 eV, significantly exceeds the electronic counterpart, 4.53 ± 0.04 eV. This result could not be easily anticipated from the previous calculations for configurations A, B, and C and points out the relevance of the liquid phase statistics. The standard deviations of the VDE distributions are obtained by multiplying the mean error by $\sqrt{80} \approx 9$, such that $\sigma$ = 0.36 eV for both the electronic and positronic detachment energies. The standard deviations indicate significant variations of the VDE values arising from the accessible solute−solvent structures in the *NpT* ensemble.

The mean VDEs computed with the APMO/P2 method are higher than the APMO/HF counterparts by 0.20 and 0.12 eV for positron and electron detachment, respectively. The decomposition of the second-order correlation energies, according to eq 8, is also shown in Table 6. The pair-


https://doi.org/10.1021/acs.jpcb.1c10124
J. Phys. Chem. B 2022, 126, 2699−2714

Table 6. Electronic ($e^-$) and Positronic ($e^+$) VDEs, in Units of Electronvolts, Computed with the APMO/HF (KT) and APMO/P2 (P2) Methods[a]

| | KT | P2 | $\mathcal{T}_{ORX}$ | $\mathcal{T}_{PRM}$ |
|---|---|---|---|---|
| $e^-$ VDE | 4.53 ± 0.04 | 4.73 ± 0.04 | − 0.79 ± 0.01 | 0.99 ± 0.01 |
| $e^+$ VDE | 5.21 ± 0.04 | 5.33 ± 0.04 | − 0.75 ± 0.01 | 0.87 ± 0.00 |
| $\tau_{Ps}$ | 6.7 ± 0.1 | | | |
| $\tau_{po}$ | 7.3 ± 0.1 | | | |
| $\tau_{co}$ | 58.0 ± 0.6 | | | |

[a]The decomposition of the correlation energy into pair-relaxation ($\mathcal{T}_{ORX}$) and -removal ($\mathcal{T}_{PRM}$) contributions and the APMO/HF annihilation lifetimes (in units of ns) are also indicated. The calculations employed scheme II for the expansion centers along with the 6-31G+(d,p)/aug-cc-pVTZ basis set (see text). The mean values and mean errors were obtained from 80 statistically uncorrelated Ps−water configurations.

Table 7. Electronic ($e^-$) and Positronic ($e^+$) VDEs (in Electronvolts) and Annihilation Lifetimes (in Nanoseconds) Obtained with the APMO/HF/6-31G++(d,p) Method for Configuration D (Reduced Cavity Model)[a]

| | oxygen centers | | ghost center | | oxygen and ghost centers | |
|---|---|---|---|---|---|---|
| | isolated | embedded | isolated | embedded | isolated | embedded |
| $e^-$ VDE | 3.38 | 3.06 | 4.85 | 4.31 | 4.20 | 3.82 |
| $e^+$ VDE | 2.60 | 3.05 | 4.08 | 4.81 | 4.16 | 5.05 |
| $\tau_{Ps}$ | 27.14 | 15.89 | 5.73 | 5.32 | 9.65 | 7.47 |
| $\tau_{po}$ | 1.89 | 2.31 | 2.10 | 2.19 | 4.55 | 5.33 |
| $\tau_{co}$ | 236.3 | 133.1 | 12.71 | 13.41 | 689.7 | 836.7 |

[a]Schemes I (oxygen centers), II (ghost center), and III (oxygen and ghost centers) for the basis set expansion were considered.

relaxation term ($\mathcal{T}_{PRX}$) was found to be negligible, while the contributions from orbital relaxation ($\mathcal{T}_{ORX}$) and pair removal ($\mathcal{T}_{PRM}$) were comparable in magnitude. These terms tend to cancel each other due to their opposite signs. Nevertheless, the pair-removal contribution, which accounts for the $e^-$−$e^-$ and $e^-$−$e^+$ correlations, exceeds the orbital relaxation term in absolute value, thus increasing the electronic and positronic binding energies with respect to the APMO/HF estimates. While the P2 correlation contributions to the VDEs are significantly higher than the mean errors, they provide modest corrections to the KT values, below 5%.

Finally, the mean annihilation lifetimes are also presented in Table 6. The statistical convergence with respect to the number of configurations is slower for the lifetimes compared to the VDEs. The relative mean errors are therefore larger for the lifetimes, and the standard deviations are $\sigma \approx 1$ ns for $\tau_{Ps}$ and $\tau_{po}$ and $\sigma \approx 5$ ns for $\tau_{co}$. The average pick-off lifetime 6.7 ns is overestimated with respect the experimental result 1.85 ns, as expected, although our result can be viewed as a lower bound for the HF-level estimate, as suggested by the comparison between schemes II and III discussed above. The pick-off lifetimes in Table 4 (see also the SI for configurations B and C) and Table 7 do not suggest significant discrepancies between the estimates obtained with the cluster and bulk models. In fact, the pick-off lifetimes obtained with scheme II and the 6-31G+(d,p)/aug-cc-pVTZ basis set for the bulk (cluster) model are 6.37 ns (5.94 ns) for configuration A, 8.51 ns (7.90 ns) for configuration B, and 5.15 ns (4.81) for configuration C. The discrepancies are also modest for the other components. For $\tau_{Ps}$ we obtained 6.33 ns (6.70 ns), 6.97 ns (7.87 ns), and 5.92 ns (6.16 ns) for configurations A, B, and C, respectively. The estimates for the core annihilation lifetimes were 54.27 ns (46.10 ns), 64.54 ns (55.45 ns), and 49.25 ns (40.56 ns) for configurations A, B, and C. While larger for the latter contribution (≈15%), the differences do not exceed 10% for the intrinsic and pick-off lifetimes. Interestingly, radial pick-off overlaps computed with the cluster and bulk models, shown in the SI, have nonzero values over essentially the same range. The results are encouraging, at least for $\tau_{po}$, despite the differences with respect to scheme III discussed above. Accurate estimates for the annihilation lifetimes will inevitably require enhancement factors, which could be tuned to compensate the errors related to less expensive computational models. In this sense, the discrepancies between schemes II and III, as well as those between the cluster and bulk models, can be viewed as reasonable.

**3.4. Reduced Cavity Size.** As explained in section 2.1, our model for hydrated Ps particles was based on a previously reported model for solvated electrons.[49] Considering the electron−oxygen RDF, the latter model predicts the cavity radius $R_0 = 2.65$ Å and the maximum of the first solvation shell $R_1 = 2.95$ Å. More recent models for hydrated electrons[58,59] point out smaller excluded volumes, with $R_0 \lesssim 2.0$ Å and $R_1 \approx 2.3$ Å.[58,59] While proposing new models for solvated electrons is beyond the scope of our work, we modified the LJ parameters to reduce the Ps excluded volume. This procedure can be viewed as more consistent with those recent theoretical accounts, but our main goal is to explore the impact of the cavity size on the physical properties of solvated Ps atoms.

By modifying the LJ parameters ($\epsilon_e = 0.16$ kcal/mol and $\sigma_e = 3.2$ Å), we obtained $R_0 = 2.35$ Å and $R_1 = 2.65$ Å for the solvated electron. The excluded volume was reduced with respect to the original model of Ludwig et al.,[49] although it is still somewhat too large. The average electron coordination number in our modified classical model, $n_C = 6$, is also overestimated with respect to other calculations,[58,59] which predict $n_C = 4$−5. Nevertheless, the modified parameters serve our purpose of exploring a modification in the cavity size. From the same procedures described in section 2.1, we obtained the LJ parameters $\epsilon_{Ps} = 0.134$ kcal/mol and $\sigma_{Ps} = 3.25$ Å for the Ps−oxygen interaction. This choice of parameters changed the repulsive $C_{12}$ coefficient, but the dispersion ($C_6$) coefficient was kept constant, i.e., the same as in the previous calculations. The Ps−oxygen RDF computed with the new set


https://doi.org/10.1021/acs.jpcb.1c10124
J. Phys. Chem. B 2022, 126, 2699−2714

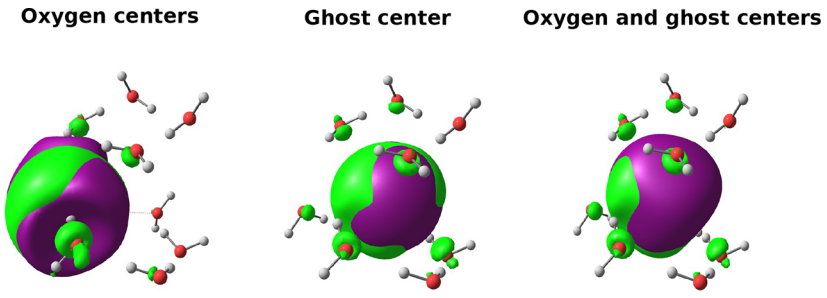


**Figure 8.** Isosurfaces of the electronic (green) and positronic (purple) SOMO orbitals obtained for configuration D (reduced cavity size) with the APMO/HF/6-31G++(d,p) method. The calculations were performed for the embedded QM clusters. Schemes I (oxygen centers), II (ghost center), and III (oxygen and ghost centers) for the basis set expansion were also considered (see text). The isovalue 0.03 au was used in all cases.

**Table 8. Electronic ($e^-$) and Positronic ($e^+$) VDEs, in Units of Electronvolts, Computed with the APMO/HF (KT) and APMO/P2 (P2) Methods for the Model with Reduced Cavity Size[a]**

| | KT | P2 | $\mathcal{T}_{ORX}$ | $\mathcal{T}_{PRM}$ |
|---|---|---|---|---|
| $e^-$ VDE | 4.54 ± 0.05 | 4.78 ± 0.04 | −0.83 ± 0.01 | 1.07 ± 0.01 |
| $e^+$ VDE | 5.23 ± 0.05 | 5.31 ± 0.04 | −0.83 ± 0.01 | 0.92 ± 0.01 |
| $\tau_{Ps}$ | 6.42 ± 0.05 | | | |
| $\tau_{po}$ | 4.71 ± 0.22 | | | |
| $\tau_{co}$ | 41.84 ± 2.02 | | | |

[a]The decomposition of the correlation energy into pair-relaxation ($\mathcal{T}_{ORX}$) and -removal ($\mathcal{T}_{PRM}$) contributions, and the APMO/HF annihilation lifetimes (in units of ns) are also indicated. The calculations employed scheme II for the expansion centers along with the 6-31G+(d,p)/aug-cc-pVTZ basis set (see text). The mean values and mean errors were obtained from 80 statistically uncorrelated Ps−water configurations.

of parameters, under the same thermodynamical conditions used in the previous calculations, is shown in Figure 1 (purple line). The Ps cavity radius was reduced by 0.2 Å, from 2.85 to 2.65 Å, while the RDF peak of the first solvation shell was downshifted from 3.75 to 3.45 Å. Bulk behavior is found beyond 10.15 Å in both Ps models. The modified model also describes Ps as a hydrophobic solute forming clathrate a structure, but the thermodynamical properties are affected by the cavity size, as expected. The solvation free energy decreases from $\Delta G_{hyd}$ = (5.58 ± 0.32) kcal/mol to $\Delta G_{hyd}$ = (2.29 ± 0.27) kcal/mol as the cavity size is reduced. The Ps−solvent energy is still small but nonzero in the modified model, $E_{Psw}$ = (−1.58 ± 0.01) kcal/mol. Unfortunately, we are not aware of experimental data for the hydration of Ps particles, which would be valuable to assess the models.

From the classical simulations, we randomly chose three statistically uncorrelated Ps−solvent configurations to obtain cluster models comprising 10 QM water molecules. As before, 140 MM solvent molecules were included to build the embedded models. Since the results obtained for those configurations were always consistent, we only show the results for one of them, referred to as configuration D (the results for another two configurations, labeled E and F, are available as SI). The positronic and electronic VDEs, along with the annihilation lifetimes, are shown in Table 7 for configuration D (see Table S10 for configurations E and F). The three schemes for the expansion centers were explored employing the APMO/HF/6-31G++(d,p) method, with and without accounting for the electrostatic embedding. We also computed VDEs and annihilation lifetimes with the reduced cavity and the 6-31G+(d,p)/aug-cc-pVXZ basis sets, where X = D, Q, and T. The latter results are available as SI, since in most of the cases the conclusions are similar to those drawn from the model discussed in sections 3.2.2 and 3.2.3. In the following, the modified set of LJ parameters will be referred to as the smaller-cavity (SC) model, while the previous set of parameters, discussed in sections 3.1−3.3, is referred to as the larger-cavity (LC) model.

Although the reduced cavity could be expected to improve scheme I, the VDEs computed without the Ps center are still discrepant (see Table 7). The SOMO isosurfaces, shown in Figure 8, corroborate the artificially displaced densities and, thus, the need to include the ghost center. The electronic VDEs computed with scheme II are generally higher than those obtained with scheme III, as in the previous calculations for the LC model (see section 3.2.2). However, the embedding tends to destabilize the electronic SOMO of configurations D, E, and F (SC model), in contrast with configurations A, B, and C (LC model). Since the RPDs of the electronic SOMOs (not shown) are similar to those shown in Figure 3, the embedding seems to increase the repulsive interaction in the model with reduced excluded volume. In general, the VDE values computed with the SC model (Tables 7 and S10) are compatible with the APMO/HF/6-31G++(d,p) calculations for configurations A, B, and C (LC model, Tables 2, S4, and S5). The VDEs obtained with the same cavity model and calculation method vary considerably among the configurations, such that no clear trend was introduced by the variation of the cavity size. We also computed ensemble averages for the VDEs employing a bulk model with 18 QM and 132 MM water molecules (scheme II for the expansion centers) and the 6-31G+(d,p)/aug-cc-pVXZ basis set. The results shown in Table 8 (SC model) can be compared with those in Table 6 (LC model), as they essentially differ by the cavity size used in the calculations. The VDE mean values are almost identical, and the standard deviations, $\sigma \approx 0.4$ eV, further indicate considerable variation among the configurations.

The annihilation lifetimes are expected to be more significantly affected by the reduced cavity size. In particular, the larger overlaps between the positronic and solvent


https://doi.org/10.1021/acs.jpcb.1c10124
J. Phys. Chem. B 2022, 126, 2699−2714

electronic densities should decrease the pick-off lifetimes (increase the pick-off rates). For the SC model, the APMO/HF/6-31G++(d,p) lifetimes are shown in Tables 7 (configuration D), S10 (configuration E), and S11 (configuration F). Although we also report the calculations for the isolated clusters, we focus the discussion on the embedded ones, for brevity. The $\tau_{Ps}$ lifetimes vary considerably among the D, E, and F configurations (SC model). The values range from 5.3 to 8.0 ns with scheme II, while they vary from 7.5 to 10.2 ns with scheme III. However, these estimates are still consistent with those obtained for configurations A, B, and C (LC model) using the 6-31G++(d,p) basis set: 6.1−7.4 ns with scheme II, and 7.9−9.4 ns with scheme III, pointing out no clear trend. The $\tau_{Ps}$ mean lifetimes for the bulk models, shown in Tables 6 and 8, differ by only 0.3 ns (5%).

For the $\tau_{po}$ lifetimes, we could find some distinction between the estimates computed with the different cavity sizes. The lifetimes obtained from scheme III and the 6-31G++(d,p) basis set are somewhat shorter for the SC model (5.3−9.0 ns) than for the LC model (7.9−11.3 ns). As discussed above, the less spherical positronic densities render the lifetimes computed with scheme III longer than those computed with scheme II. However, the differences are more significant for the SC model with the 6-31G++(d,p) basis set. When employed along with scheme II for the expansion centers, the latter basis provides unexpectedly short lifetimes, ranging from 2.2 to 2.7 ns for configurations D, E, and F (SC model). These values are close to those computed with scheme I, employing either cavity, which spuriously agrees with the experimental data, as discussed in section 2.3. Nonetheless, the 6-31G+(d,p)/aug-cc-pVXZ basis sets combined with scheme II (see Tables S12 and S13) increase the pick-off lifetimes for configurations D, E, and F (3.6−9.0 ns), pointing out a limitation of the 6-31G++(d,p) set. The mean $\tau_{po}$ lifetime of the SC bulk model (4.71 ns) differs from the mean value computed with the LC model (7.25 ns), as shown in Tables 6 and 8. The shorter lifetime obtained with the smaller cavity could be viewed as an improvement, since the experimental value is 1.85 ns. However, the theoretical results should be considered with caution. The bulk models used scheme II, which tends to overestimated the density overlaps due to the more spherical positronic orbitals, compared to scheme III. In addition, the estimates for the A−C (LC) and D−F (SC) configurations suggest smaller differences between the cavity models in the case when scheme III is employed. One should bear in mind the inherent limitations to the annihilation rates computed with the HF method, such that consistent calculations should be in disagreement with the experiment. These limitations can be overcome with empirical corrections, such that we consider the $\tau_{po}$ estimates obtained with both cavity models equivalent in practical terms.

Finally, the contribution from the core orbitals to the pick-off rates is more sensitive to the calculation method, as already pointed out. If we consider scheme III along with the 6-31G++(d,p) basis set, the SC model provides shorter $\tau_{co}$ lifetimes compared to the previous model, roughly by a factor of 2. The differences between the results obtained with schemes II and III are smaller for the reduced cavity, although still huge. The $\tau_{co}$ lifetime is the most sensitive property with respect to the expansion center schemes and basis sets, and it is also impacted by the change in cavity size. This is not a stringent limitation to the computation of the pick-off lifetimes in view of the modest contribution from the core orbitals, but core annihilation lifetimes seem to be the most challenging calculations.

## 4. CONCLUSIONS AND PERSPECTIVES

We have proposed a QM/MM model for solvated Ps atoms in water, exploring classical MC simulations and APMO quantum calculations. The classical FF for Ps atoms can be readily obtained from the combination of a solvated electron model (repulsive part) and a Slater−Kirkwood approach to the dispersion constant. Our protocol is general in the sense that it can be applied to other liquids and materials. Reliable FFs are available for a large variety of systems, so one would basically need to describe the solvated electron in the environment of interest.

The thermodynamical properties obtained from the MC simulations point out similarities between the solvation of Ps and noble gas atoms, hydrophobic solutes that form clathrate structures. The QM calculations indicate that the choice of basis set deserves attention. The relatively small 6-31G+(d,p) basis set produced poor results, in disagreement with those obtained from more robust basis sets. However, our calculations indicate a mild dependence of several properties (total energies, VDEs, and RPDs) on the basis sets, as long as they are large and diffuse enough. The expansion centers also play a relevant role. The attempt to expand the wave function only from the atomic centers produced poor results. The convergence of the total energy with respect to the basis set size was very slow, giving rise to positron densities artificially shifted from the solute cavity into the solvent. Additional electronic and positronic basis functions on the ghost center corresponding to the Ps position in the MC simulations significantly improved the total energies. We compared APMO/HF calculations employing a single expansion center for the positronic wave function with a multicenter expansion. As long as the total energies, VDEs, and radial distributions are concerned, the discrepancies between the two schemes are tolerable, making the single-center expansion attractive in view of the lower computational cost.

The numerical tests were carried out for relatively small QM clusters, but we also considered thermodynamical averages for a system comprising 80 solute−solvent configurations with 22 solvent molecules in the QM region, corresponding to the first solvation shell. This larger model is expected to account for the properties of solvated Ps atoms in liquid water. The calculated mean detachment energies were significantly larger for the positronic SOMO, compared to the electronic counterpart. We further explored second-order correlation effects for the bulk model, and they were found to increase the VDE values by approximately 5% with respect to the KT estimates.

While our main goal was to propose the QM/MM protocol and explore the structural, thermodynamical, and numerical aspects outlined above, we also considered annihilation lifetimes, discriminating the direct, pick-off, and core contributions. The APMO/HF wave functions do not provide a quantitative description of annihilation, as expected, but they were useful to shed light on some numerical aspects. The discrepancies among different basis sets or expansion schemes are generally larger for the annihilation lifetimes, compared to the VDEs. This was particularly true for calculations performed with the single-center and multicenter expansions using robust basis sets. The single-center positronic orbitals are nearly spherically symmetric, in contrast to the orbitals obtained from the multicenter expansion, thus impacting the pick-off rates.



https://doi.org/10.1021/acs.jpcb.1c10124
J. Phys. Chem. B 2022, 126, 2699−2714

The quantitative description of the annihilation process, resorting to either enhancement factors or empirical corrections, will be the subject of future work.

We further explored a model with reduced cavity size. The VDEs and direct annihilation lifetime were rather insensitive to the change in cavity size. The pick-off lifetime is more significantly affected by the cavity model, as expected. The smaller cavity favors the positron−solvent density overlaps and, thus, provides smaller $\tau_{po}$ values. Nevertheless, empirical corrections to the HF-level annihilation rates are always necessary, regardless of the cavity size, so the conclusions drawn from both cavity models are basically the same.

## ■ ASSOCIATED CONTENT

### Supporting Information

The Supporting Information is available free of charge at https://pubs.acs.org/doi/10.1021/acs.jpcb.1c10124.

Additional details about classical simulations results. Total energies, vertical detachment energies, radial probability densities, isosurfaces, annihilation lifetimes, and radial pick-off overlap for configurations B, C, E, and F (PDF)

## ■ AUTHOR INFORMATION


### Corresponding Author

**Márcio T. do N. Varella** − *Instituto de Física, Universidade de São Paulo, 05508-090 São Paulo, SP, Brazil;* orcid.org/0000-0002-5812-0342; Email: mvarella@if.usp.br

### Authors

**Mateus Bergami** − *Instituto de Física, Universidade de São Paulo, 05508-090 São Paulo, SP, Brazil*

**Andre L. D. Santana** − *Instituto de Física, Universidade de São Paulo, 05508-090 São Paulo, SP, Brazil*

**Jorge Charry Martinez** − *Department of Physics and Materials Science, University of Luxembourg, L-1511 Luxembourg City, Luxembourg;* orcid.org/0000-0003-3069-2522

**Andres Reyes** − *Department of Chemistry, Universidad Nacional de Colombia, 111321 Bogotá, Colombia;* orcid.org/0000-0001-7571-2078

**Kaline Coutinho** − *Instituto de Física, Universidade de São Paulo, 05508-090 São Paulo, SP, Brazil;* orcid.org/0000-0002-7586-3324

Complete contact information is available at: https://pubs.acs.org/10.1021/acs.jpcb.1c10124


### Notes

The authors declare no competing financial interest.

## ■ ACKNOWLEDGMENTS

M.B. acknowledges support from the Brazilian agency Coordenação de Aperfeiçoamento de Pessoal de Nível Superior (CAPES). M.T.N.V. acknowledges support from the National Council for Scientific and Technological Development (CNPq), grant no. 304571/2018-0. The calculations were partly performed with HPC resources from STI (University of São Paulo). K.C. acknowledges support from CNPq, CAPES, and FAPESP, grant no. 2021/09016-3.

## ■ REFERENCES


(1) Čížek, J. Characterization of lattice defects in metallic materials by positron annihilation spectroscopy: A review. *Journal of Materials Science & Technology* **2018**, *34*, 577−598.

(2) Krause-Rehberg, R.; Leipner, H. S. *Positron annihilation in semiconductors: defect studies*; Springer Science & Business Media, 1999.

(3) Pethrick, R. A. Positron annihilation—a probe for nanoscale voids and free volume? *Prog. Polym. Sci.* **1997**, *22*, 1−47.

(4) Sharma, S.; Pujari, P. Role of free volume characteristics of polymer matrix in bulk physical properties of polymer nanocomposites: A review of positron annihilation lifetime studies. *Prog. Polym. Sci.* **2017**, *75*, 31−47.

(5) Zubiaga, A.; Warringham, R.; Boltz, M.; Cooke, D.; Crivelli, P.; Gidley, D.; Pérez-Ramírez, J.; Mitchell, S. The assessment of pore connectivity in hierarchical zeolites using positron annihilation lifetime spectroscopy: instrumental and morphological aspects. *Phys. Chem. Chem. Phys.* **2016**, *18*, 9211−9219.

(6) Singh, A. N. Positron annihilation spectroscopy in tomorrow's material defect studies. *Appl. Spectrosc. Rev.* **2016**, *51*, 359−378.

(7) Maheshwari, P.; Gorgol, M.; Kierys, A.; Zaleski, R. Positron Probing of Liquid-free Volume To Investigate Adsorption−Desorption Behavior of Water in Two-Dimensional Mesoporous SBA-3. *J. Phys. Chem. C* **2017**, *121*, 17251−17262.

(8) Jean, Y. C.; Mallon, P. E.; Schrader, D. M. *Principles and Applications of Positron and Positronium Chemistry*; World Scientific: Singapore, 2003.

(9) Gidley, D. W.; Peng, H.-G.; Vallery, R. S. Positron annihilation as a method to characterize porous materials. *Annu. Rev. Mater. Res.* **2006**, *36*, 49−79.

(10) Chen, H. M.; Van Horn, J. D.; Jean, Y. C. Applications of positron annihilation spectroscopy to life science. *Defect and diffusion forum* **2012**, *331*, 275−293.

(11) Fong, C.; Dong, A. W.; Hill, A. J.; Boyd, B. J.; Drummond, C. J. Positron annihilation lifetime spectroscopy (PALS): a probe for molecular organisation in self-assembled biomimetic systems. *Phys. Chem. Chem. Phys.* **2015**, *17*, 17527−17540.

(12) García-Arribas, A. B.; Axpe, E.; Mujika, J. I. n.; Mérida, D.; Busto, J. V.; Sot, J.; Alonso, A.; Lopez, X.; García, J. A.; Ugalde, J. M.; et al. Cholesterol−ceramide interactions in phospholipid and sphingolipid bilayers as observed by positron annihilation lifetime spectroscopy and molecular dynamics simulations. *Langmuir* **2016**, *32*, 5434−5444.

(13) Dong, A. W.; Fong, C.; Waddington, L. J.; Hill, A. J.; Boyd, B. J.; Drummond, C. J. Application of positron annihilation lifetime spectroscopy (PALS) to study the nanostructure in amphiphile self-assembly materials: phytantriol cubosomes and hexosomes. *Phys. Chem. Chem. Phys.* **2015**, *17*, 1705−1715.

(14) Chieng, N.; Cicerone, M. T.; Zhong, Q.; Liu, M.; Pikal, M. J. Characterization of dynamics in complex lyophilized formulations: II. Analysis of density variations in terms of glass dynamics and comparisons with global mobility, fast dynamics, and Positron Annihilation Lifetime Spectroscopy (PALS). *Eur. J. Pharm. Biopharm.* **2013**, *85*, 197−206.

(15) Muehllehner, G.; Karp, J. S. Positron emission tomography. *Physics in Medicine & Biology* **2006**, *51*, R117.

(16) Weber, W. A. Positron emission tomography as an imaging biomarker. *Journal of Clinical Oncology* **2006**, *24*, 3282−3292.

(17) Jones, T.; Townsend, D. W. History and future technical innovation in positron emission tomography. *Journal of Medical Imaging* **2017**, *4*, 011013.

(18) Stepanov, P. S.; Selim, F. A.; Stepanov, S. V.; Bokov, A. V.; Ilyukhina, O. V.; Duplâtre, G.; Byakov, V. M. Interaction of positronium with dissolved oxygen in liquids. *Phys. Chem. Chem. Phys.* **2020**, *22*, 5123−5131.

(19) Shibuya, K.; Saito, H.; Nishikido, F.; Takahashi, M.; Yamaya, T. Oxygen sensing ability of positronium atom for tumor hypoxia imaging. *Communications Physics* **2020**, *3*, 1−8.

(20) Kacperski, K.; Spyrou, N. M.; Smith, F. A. Three-gamma annihilation imaging in positron emission tomography. *IEEE transactions on medical imaging* **2004**, *23*, 525−529.
(21) Moskal, P.; Kisielewska, D.; Curceanu, C.; Czerwiński, E.; Dulski, K.; Gajos, A.; Gorgol, M.; Hiesmayr, B.; Jasińska, B.; Kacprzak, K.; et al. Feasibility study of the positronium imaging with the J-PET tomograph. *Physics in Medicine & Biology* **2019**, *64*, 055017.
(22) White, R. D.; Tattersall, W.; Boyle, G.; Robson, R. E.; Dujko, S.; Petrovic, Z. L.; Bankovic, A.; Brunger, M. J.; Sullivan, J. P.; Buckman, S. J.; et al. Low-energy electron and positron transport in gases and soft-condensed systems of biological relevance. *Applied Radiation and Isotopes* **2014**, *83*, 77−85.
(23) Solov'yov, A. V. *Nanoscale insights into ion-beam cancer therapy*; Springer, 2016.
(24) Moadel, R. M.; Weldon, R. H.; Katz, E. B.; Lu, P.; Mani, J.; Stahl, M.; Blaufox, M. D.; Pestell, R. G.; Charron, M. J.; Dadachova, E. Positherapy: targeted nuclear therapy of breast cancer with 18F-2-deoxy-2-fluoro-D-glucose. *Cancer Res.* **2005**, *65*, 698−702.
(25) Hioki, T.; Gholami, Y. H.; Katz, K. J.; McKelvey; Aslani, A.; Marquis, H.; Eslick, E. M.; Willowson, K. P.; Howell, V. M.; Bailey, D. L. Overlooked potential of positrons in cancer therapy. *Sci. Rep.* **2021**, *11*, 2475.
(26) Solov'yov, A. V.; Surdutovich, E.; Scifoni, E.; Mishustin, I.; Greiner, W. Physics of ion beam cancer therapy: a multiscale approach. *Phys. Rev. E* **2009**, *79*, 011909.
(27) Robson, R. E.; Brunger, M. J.; Buckman, S. J.; Garcia, G.; Petrović, Z. L.; White, R. D. Positron kinetics in an idealized PET environment. *Sci. Rep.* **2015**, *5*, 1−10.
(28) Stepanov, S. V.; Byakov, V. M.; Zvezhinskiy, D. S.; Duplâtre, G.; Nurmukhametov, R. R.; Stepanov, P. S. Positronium in a liquid phase: formation, bubble state and chemical reactions. *Adv. Phys. Chem.* **2012**, *2012*, 431962.
(29) Stepanov, S. V.; Byakov, V.; Zvezhinskiy, D.; Duplâtre, G. Enegertics of the Ps Formation: Role of the Solvated Electron. *Defect and Diffusion Forum* **2017**, *373*, 17−22.
(30) Castellaz, P.; Siegle, A.; Stoll, H. Positron age-momentum-correlation (AMOC) measurements on organic liquids. *Journal of Nuclear and Radiochemical Sciences* **2002**, *3*, R1−R7.
(31) Jasińska, B.; Zgardzińska, B.; Chołubek, G.; Pietrow, M.; Gorgol, M.; Wiktor, K.; Wysoglad, K.; Białas, P.; Curceanu, C.; Czerwiński, E.; et al. Human tissue investigations using PALS technique: free radicals influence. *Acta Phys. Polym., A* **2017**, *132*, 1556−1558.
(32) Stepanov, S. V.; Zvezhinskiy, D.; Duplâtre, G.; Byakov, V.; Batskikh, Y. Y.; Stepanov, P. S. Incorporation of the magnetic quenching effect into the blob model of Ps formation. Finite sized Ps in a potential well. *Mater. Sci. Forum* **2010**, *666*, 109−114.
(33) Ferrell, R. A. Long Lifetime of Positronium in Liquid Helium. *Phys. Rev.* **1957**, *108*, 167−168.
(34) Tao, S. J. Positronium Annihilation in Molecular Substances. *J. Chem. Phys.* **1972**, *56*, 5499−5510.
(35) Eldrup, M.; Lightbody, D.; Sherwood, J. N. The temperature dependence of positron lifetimes in solid pivalic acid. *Chem. Phys.* **1981**, *63*, 51−58.
(36) Stepanov, S. V.; Zvezhinskiy, D. S.; Byakov, V. M. Beyond the point ps approximation. *Mater. Sci. Forum* **2012**, *733*, 7−14.
(37) Zgardzińska, B. The size of smallest subnanometric voids estimated by positron annihilation method. Correction to the Tao-Eldrup model. *Chem. Phys. Lett.* **2015**, *622*, 20−22.
(38) Tanzi Marlotti, G; Consolati, G; Castelli, F Formal calculation of exchange correlation effects on annihilation lifetimes of positronium confined in small cavities. *J. Phys.: Condens. Matter* **2020**, *32*, 025602.
(39) Chuev, G. N.; Schrader, D. M.; Stepanov, S. V.; Byakov, V. M. Quantum mechanics of solvated complexes: A test for positronium. *Int. J. Quantum Chem.* **2002**, *88*, 634−641.
(40) Chuev, G. N. Integral equation treatment of solvated quantum particles. *J. Mol. Liq.* **2003**, *105*, 161−164.
(41) Schmitz, H.; Müller-Plathe, F. Calculation of the lifetime of positronium in polymers via molecular dynamics simulations. *J. Chem. Phys.* **2000**, *112*, 1040−1045.
(42) Larrimore, L.; McFarland, R.; Sterne, P.; Bug, A. L. A two-chain path integral model of positronium. *J. Chem. Phys.* **2000**, *113*, 10642−10650.
(43) Miller, B. N.; Reese, T. Path integral simulation of positronium. *Nuclear Instruments and Methods in Physics Research Section B: Beam Interactions with Materials and Atoms* **2002**, *192*, 176−179.
(44) Bug, A. L.; Sterne, P. Path integral Monte Carlo simulations of positronium annihilation: From micropores to mesopores. *Phys. Rev. B* **2006**, *73*, 094106.
(45) Bug, A. L.; Cronin, T. W.; Sterne, P.; Wolfson, Z. S. Simulation of positronium: Toward more realistic models of void spaces in materials. *Radiat. Phys. Chem.* **2007**, *76*, 237−242.
(46) Tachikawa, M.; Kita, Y.; Buenker, R. J. Bound states of the positron with nitrile species with a configuration interaction multi-component molecular orbital approach. *Phys. Chem. Chem. Phys.* **2011**, *13*, 2701−2705.
(47) Reyes, A.; Moncada, F.; Charry, J. The any particle molecular orbital approach: A short review of the theory and applications. *Int. J. Quantum Chem.* **2019**, *119*, No. e25705.
(48) Coutinho, K.; Canuto, S. Solvent Effects from a Sequential Monte Carlo - Quantum Mechanical Approach. *Adv. Quantum Chem.* **1997**, *28*, 89−105.
(49) Ludwig, V.; Coutinho, K.; Canuto, S. Sequential classical-quantum description of the absorption spectrum of the hydrated electron. *Phys. Rev. B* **2004**, *70*, 214110.
(50) Blanco, F.; Roldán, A.; Krupa, K.; McEachran, R.; White, R.; Marjanović, S.; Petrović, Z. L.; Brunger, M. J.; Machacek, J.; Buckman, S. J.; et al. Scattering data for modelling positron tracks in gaseous and liquid water. *Journal of Physics B: Atomic, Molecular and Optical Physics* **2016**, *49*, 145001.
(51) Incerti, S.; Kyriakou, I.; Bernal, M.; Bordage, M.-C.; Francis, Z.; Guatelli, S.; Ivanchenko, V.; Karamitros, M.; Lampe, N.; Lee, S. B.; et al. Geant4-DNA example applications for track structure simulations in liquid water: A report from the Geant4-DNA Project. *Med. Phys.* **2018**, *45*, e722−e739.
(52) Schuemann, J.; McNamara, A.; Ramos-Méndez, J.; Perl, J.; Held, K.; Paganetti, H.; Incerti, S.; Faddegon, B. TOPAS-nBio: an extension to the TOPAS simulation toolkit for cellular and sub-cellular radiobiology. *Radiation research* **2019**, *191*, 125−138.
(53) Cezar, H. M.; Canuto, S.; Coutinho, K. DICE: A Monte Carlo Code for Molecular Simulation Including the Configurational Bias Monte Carlo Method. *J. Chem. Inf. Model.* **2020**, *60*, 3472−3488.
(54) Berendsen, H. J. C.; Grigera, J. R.; Straatsma, T. P. The missing term in effective pair potentials. *J. Phys. Chem.* **1987**, *91*, 6269−6271.
(55) Tkatchenko, A.; Scheffler, M. Accurate Molecular Van Der Waals Interactions from Ground-State Electron Density and Free-Atom Reference Data. *Phys. Rev. Lett.* **2009**, *102*, 073005.
(56) Martin, D.; Fraser, P. The van der Waals force between positronium and light atoms. *Journal of Physics B: Atomic and Molecular Physics* **1980**, *13*, 3383.
(57) Johnson, R. D., III, Ed. *NIST Computational Chemistry Comparison and Benchmark Database, NIST Standard Reference Database Number 101, Release 21*; NIST, 2020.
(58) Herbert, J. M. Structure of the aqueous electron. *Phys. Chem. Chem. Phys.* **2019**, *21*, 20538−20565.
(59) Lan, J.; Kapil, V.; Gasparotto, P.; Ceriotti, M.; Iannuzzi, M.; Rybkin, V. V. Simulating the ghost: quantum dynamics of the solvated electron. *Nat. Commun.* **2021**, *12*, 1−6.
(60) Flores-Moreno, R.; Posada, E.; Moncada, F.; Romero, J.; Charry, J.; Díaz-Tinoco, M.; González, S. A.; Aguirre, N. F.; Reyes, A. LOWDIN: The any particle molecular orbital code. *Int. J. Quantum Chem.* **2014**, *114*, 50−56.
(61) Charry, J.; Romero, J.; Varella, M. T. d. N.; Reyes, A. Calculation of positron binding energies of amino acids with the any-particle molecular-orbital approach. *Phys. Rev. A* **2014**, *89*, 052709.


https://doi.org/10.1021/acs.jpcb.1c10124
J. Phys. Chem. B 2022, 126, 2699−2714

(62) Romero, J.; Charry, J. A.; Flores-Moreno, R.; Varella, M. T. d. N.; Reyes, A. Calculation of positron binding energies using the generalized any particle propagator theory. *J. Chem. Phys.* **2014**, *141*, 114103.
(63) Lu, T.; Chen, F. Multiwfn: A multifunctional wavefunction analyzer. *J. Comput. Chem.* **2012**, *33*, 580−592.
(64) Robles, J. C.; Ogando, E.; Plazaola, F. Positron lifetime calculation for the elements of the periodic table. *J. Phys.: Condens. Matter* **2007**, *19*, 176222.
(65) Barbiellini, B.; Kuriplach, J. Proposed parameter-free model for interpreting the measured positron annihilation spectra of materials using a generalized gradient approximation. *Physical review letters* **2015**, *114*, 147401.
(66) Fraser, P. Positrons and Positronium in Gases. *Advances in Atomic and Molecular Physics*; Academic Press, 1968; Vol. *4*; pp 63−107.
(67) Ryzhikh, G.; Mitroy, J. Positron annihilation profiles for HPs and He (3Se) e+. *Journal of Physics B: Atomic, Molecular and Optical Physics* **1999**, *32*, 4051.
(68) Becke, A. D. A multicenter numerical integration scheme for polyatomic molecules. *J. Chem. Phys.* **1988**, *88*, 2547−2553.
(69) Zwanzig, R. W. High-temperature equation of state by a perturbation method. I. Nonpolar gases. *J. Chem. Phys.* **1954**, *22*, 1420−1426.
(70) Jorgensen, W. L.; Ravimohan, C. Monte Carlo simulation of differences in free energies of hydration. *J. Chem. Phys.* **1985**, *83*, 3050−3054.
(71) Georg, H. C.; Coutinho, K.; Canuto, S. A look inside the cavity of hydrated a-cyclodextrin: A computer simulation study. *Chem. Phys. Lett.* **2005**, *413*, 16−21.
(72) Straatsma, T. P.; Berendsen, H. J. C.; Postma, J. P. M. Free energy of hydrophobic hydration: A molecular dynamics study of noble gases in water. *J. Chem. Phys.* **1986**, *85*, 6720−6727.
(73) Guedes, R. C.; Coutinho, K.; Cabral, B. J. C.; Canuto, S.; Correia, C. F.; dos Santos, R. M. B.; Martinho Simões, J. A. Solvent Effects on the Energetics of the Phenol O-H Bond: Differential Solvation of Phenol and Phenoxy Radical in Benzene and Acetonitrile. *J. Phys. Chem. A* **2003**, *107*, 9197−9207.
(74) Haselmeier, R.; Holz, M.; Marbach, W.; Weingaertner, H. Water Dynamics near a Dissolved Noble Gas. First Direct Experimental Evidence for a Retardation Effect. *J. Phys. Chem.* **1995**, *99*, 2243−2246.
(75) Canuto, S.; Coutinho, K. From Hydrogen Bond to Bulk: Solvation Analysis of the $n - \pi^*$ Transition of Formaldehyde in Water. *Int. J. Quantum Chem.* **2000**, *77*, 192−198.
(76) Barreto, R. C.; Coutinho, K.; Georg, H. C.; Canuto, S. Combined Monte Carlo and quantum mechanics study of the solvatochromism of phenol in water. The origin of the blue shift of the lowest $\pi$-$\pi^*$ transition. *Phys. Chem. Chem. Phys.* **2009**, *11*, 1388−1396.
(77) Frigato, T.; VandeVondele, J.; Schmidt, B.; Schütte, C.; Jungwirth, P. Ab initio molecular dynamics simulation of a medium-sized water cluster anion: From an interior to a surface-located excess electron via a delocalized state. *J. Phys. Chem. A* **2008**, *112*, 6125−6133.
(78) Siefermann, K. R.; Liu, Y.; Lugovoy, E.; Link, O.; Faubel, M.; Buck, U.; Winter, B.; Abel, B. Binding energies, lifetimes and implications of bulk and interface solvated electrons in water. *Nature Chem.* **2010**, *2*, 274−279.
(79) Nummela, M.; Raebiger, H.; Yoshida, D.; Tachikawa, M. Positron binding properties of glycine and its aqueous complexes. *J. Phys. Chem. A* **2016**, *120*, 4037−4042.
(80) Elkins, M. H.; Williams, H. L.; Shreve, A. T.; Neumark, D. M. Relaxation mechanism of the hydrated electron. *Science* **2013**, *342*, 1496−1499.
(81) Gribakin, G.; Ludlow, J. Many-body theory of positron-atom interactions. *Phys. Rev. A* **2004**, *70*, 032720.
(82) Strasburger, K.; Chojnacki, H. On the reliability of the SCF and CI wavefunctions for systems containing positrons. *Chemical Physics Letters* **1995**, *241*, 485−489.





https://doi.org/10.1021/acs.jpcb.1c10124
J. Phys. Chem. B 2022, 126, 2699−2714